MSP1 **encodes an essential RNA-binding PPR factor required for** ***nad1*** **maturation and complex I biogenesis in** ***Arabidopsis*** **mitochondria**

Corinne Best[1,§], Ron Mizrahi[1,§], Rana Edris[1], Hui Tang[2], Hagit Zer[1], Catherine Colas des Francs-Small[3], Omri M. Finkel[1], Hongliang Zhu[2], Ian D. Small[3], Oren Ostersetzer-Biran[1,*]

[1] Department of Plant and Environmental Sciences, The Alexander Silberman Institute of Life Sciences, The Hebrew University of Jerusalem, Jerusalem, 91904, Israel.
[2] College of Food Science & Nutritional Engineering, China Agricultural University, Beijing 100083, China.
[3] Australian Research Council Centre of Excellence in Plant Energy Biology, School of Molecular Sciences, The University of Western Australia, 35 Stirling Highway, Crawley, WA 6009, Australia.

[§] - These authors have equally contributed to the MS

*Address correspondence to Oren Ostersetzer-Biran. Tel. +972-2-658-5191; Fax, +972-2-658-5191; *E-mail*, oren.ostersetzer@mail.huji.ac.il;

Running title: MSP1 mediates *nad1.1* pre-RNA 3'-end processing

Abstract

Mitochondria are semi-autonomous organelles that serve as hubs for aerobic energy metabolism. The biogenesis of the respiratory (OXPHOS) system relies on nuclear-encoded factors, which regulate the transcription, processing and translation of mitochondrial (mt)RNAs. These include proteins of primordial origin, as well as eukaryotic-type RNA-binding families recruited from the host genomes to function in mitogenome expression. Pentatricopeptide repeat (PPR) proteins constitute a major gene-family in angiosperms that is pivotal in many aspects of mtRNA metabolism, such as editing, splicing or stability. Here, we report the analysis of *MITOCHONDRIA STABILITY/PROCESSING PPR FACTOR1* (*MSP1*, At4g20090), a canonical mitochondria-localized PPR protein that is necessary for mitochondrial biogenesis and embryo-development. Functional complementation confirmed that the phenotypes result from a disruption of the *MSP1* gene. As a loss-of-function allele of *Arabidopsis MSP1* leads to seed abortion, we employed an embryo-rescue method for the molecular characterization of *msp1* mutants. Our data show that *msp1* embryo-development fails to proceed beyond the heart-torpedo transition stage as a consequence of a severe *nad1* pre-RNA processing-defect, resulting in the loss of respiratory complex I (CI) activity. The maturation of *nad1* involves the processing of three RNA-fragments, *nad1.1*, *nad1.2* and *nad1.3*. Based on detailed analyses of the mtRNA profiles in wild-type and *msp1* plants, we concluded that through its association with a specific site in *nad1.1*, MSP1 facilitates the generation of its 3'-terminus and stabilizes it - a prerequisite for *nad1* exons a-b splicing. Our data substantiate the importance of mtRNA metabolism for the biogenesis of the respiratory machinery during early-plant development.

Introduction

Mitochondria serve as hubs for cellular metabolism. In non-photosynthetic cells, they generate most of the energy used in the biochemical reactions required to sustain growth and development. As descendants of a symbiotic bacterium, most mitochondria harbor an intrinsic genetic system (mtDNA, or mitogenome) to make their own RNAs and proteins. Nevertheless, the majority of their proteins (Fuchs et al., 2020; Senkler et al., 2017) and some tRNAs (Salinas-Giegé et al., 2015) are encoded in the nucleus and imported into the organelle. The biogenesis of the oxidative phosphorylation (OXPHOS) system in plants (Millar et al., 2011; Schertl and Braun, 2014) is a multifaceted process, which relies on complex regulatory mechanisms to allow the stoichiometric accumulation of subunits encoded by the two separate genome machineries (Best et al., 2020a; Schwarzländer et al., 2012; Woodson and Chory, 2008). Despite their universal role in eukaryotic cells, various important aspects distinguish the mitogenomes of land plants from those in animals. While the mtDNA in mammals, or humans, underwent extensive compaction (to ~15–18 kb), their counterparts in angiosperms are notably larger in size (168 up to 11,000 kb) (Sloan et al., 2012) and much more complex in structure (Gualberto and Newton, 2017). Accumulating data suggest that mitochondrial RNA (mtRNA) processing plays a pivotal role in the regulation of mitochondria gene-expression in land plants (Best *et al.*, 2020a). For example, many essential genes in angiosperm mitochondria harbor introns, which must be excised post-transcriptionally from the pre-mRNAs to allow the integration of exons into functional reading frames (Zmudjak and Ostersetzer-Biran, 2017). These are primarily found in NADH-dehydrogenase (CI) genes, but also interrupt the coding-sequences of cytochrome *c* oxidase (CIV), cytochrome *c* biogenesis (CCM) or ribosomal protein-coding genes. These are mainly group II introns (Bonen, 2008), an ancient class of catalytic RNAs that are evolutionarily related to nuclear spliceosomal RNAs, non-LTR retrotransposons and telomerases (Lambowitz and Belfort, 2015). It is therefore speculated that the symbiont introns had a major role in shaping the genomic organization of terrestrial life forms, and may have also been determining factors in the rise of the nuclear envelope, in order to separate transcription from translation (Martin and Koonin, 2006).

Group II introns are characterized by six domains (D1-D6) based on secondary structure, which adopt a complex tertiary structure mediated by long-range tertiary interactions (Zhao and Pyle, 2017). Canonical introns in this class are able to catalyze their own excision in-vitro, but their activities in-vivo rely on intron-encoded proteins (*i.e.*, maturase, Pfam-01348), which assist

in the folding of their cognate introns into the catalytically-active form (Mizrahi et al., 2022; Zhao and Pyle, 2017). The mitochondrial introns in angiosperms have diverged considerably in sequence and have usually also lost their cognate maturase-ORFs (Guo and Mower, 2013; Schmitz-Linneweber et al., 2015). Some are fragmented, requiring the intron parts to be transcribed independently and then to associate non-covalently allowing splicing in '*trans*' (Bonen, 2008). During evolution, land plants have acquired many host factors to assist in the splicing of their highly derived organellar introns (Brown et al., 2014; Zmudjak and Ostersetzer-Biran, 2017). A few are related to maturases (Pfam-01348)(Mizrahi *et al.*, 2022), but most belong to a diverse set of RNA-binding protein families, such as RNA-helicases (pfam-00270), mitochondrial transcription termination factors (mTERFs, Pfam-02536), plant organelle RNA recognition (PORR, Pfam-11955), and pentatricopeptide repeat (PPR, Pfam-13812) proteins (Zmudjak and Ostersetzer-Biran, 2017). Currently there is very little mechanistic information about the molecular functions of these factors, specifically how they facilitate the processing of their mtRNA targets.

PPR proteins comprise one of the largest known protein families in angiosperms, with ~450 members in *Arabidopsis* (Small and Peeters, 2000). These contain between 2 and 30 repeats of a 35-amino-acid domain, which adopts an 'antiparallel' helical form (Gully et al., 2015; Shen et al., 2015), and can be classified according to variations in their PPR motifs (Lurin et al., 2004). Most plant PPRs contain N-terminal signals that target them to the 'energy-producing' organelles, where they affect diverse RNA-processing steps, including stability, trimming, editing and splicing (Barkan and Small, 2014). These act as sequence-specific ssRNA-binding proteins, where the RNA winds around the protein, by a mechanism like that by which transcription activator-like effectors (TALEs) bind dsDNA (Barkan et al., 2012; Yagi et al., 2013). In this work, we elucidate the roles of a P-class PPR protein encoded by the *AT4G20090* gene. In accordance with its role in mtRNA processing, we have renamed this gene *MITOCHONDRIA STABILITY/PROCESSING PPR FACTOR1* (*MSP1*). By studying the physiology of previously unattainable *msp1* knockout-lines, we demonstrate the effects of MSP1 on mitochondria gene-expression and function.

Results

AT4G20090 encodes a canonical P-class PPR protein

Considering the importance of mtRNA metabolism for embryo-development and plant physiology, we surveyed the *Arabidopsis* SeedGene/EMB databases (Meinke, 2020), which include ~2,200 embryogenesis mutants. Among these, 35 are identified as PPRs, 19 of which are known or predicted to reside in the mitochondria (Table 1, Table S1). These include APPR6 (Manavski et al., 2012), COD1 (Dahan et al., 2014), DEK36 (Wang et al., 2017) and OTP43 (Falcon de Longevialle et al., 2007) that function in mtRNA processing. Here, we report the characterization of MSP1/EMB1025, a P-class PPR whose functions are essential during early embryogenesis (Table 1).

Gene-expression databases (Berardini et al., 2015; Hruz et al., 2008) indicate that *MSP1* (Fig. 1A) is a lowly-expressed gene, showing most expression in embryonic and young-developing tissues (Fig. S1). Prediction of conserved motifs indicate that MSP1 (660 aa) harbors at least 11 PPR motifs (Fig. 1A), with a suggested topology of: NH_2-76aa-(P)-(P)-(P)-P-P-P-P-P-P-P-P-P-P-P-(P)-50aa-COOH, with lower scores for the first three and last PPR motifs (Figs. 1A, S2A). The AlphaFold algorithm (Jumper et al., 2021) suggests a typical PPR-fold for MSP1 (Fig. S2B), with right-handed two-turn superhelical structure. Based on this model, the 11 well-supported PPR motifs of MSP1 are bounded by an undefined structure at the N'-terminus, which comprises of the 36/37 amino-acid organellar localization signal and the first three PPR-like motifs, and a low confidence region within the C-terminus that may contain an additional PPR motif (Fig. S2B).While the PPR domains confer sequence-specific RNA recognition, the low complexity regions may contribute to protein-protein or protein-ligand interactions, as also shown for the superhelix TPR or TALE repeat proteins (Deng et al., 2012; Grove et al., 2008). Like PPR10 (Gully *et al.*, 2015; Yin et al., 2013), the internal core of MSP1 harbors a basic surface (Figs. S2B), which is postulated to represent an RNA-binding path. However, functional analyses were required to test the predicted RNA-binding characteristics of MSP1.

MSP1 is located within the mitochondria, *in-vivo*

The N-terminal region of MSP1 shares homology with the consensus sequences of mitochondrial targeting signals (Fig. S2A, Table 1). This was also supported by global confocal microscopy-based GFP-fusions of *Arabidopsis* proteins (Lurin *et al.*, 2004). To further confirm the intracellular location of MSP1, constructs encoding the plastidial Rubisco small subunit (RbcS) (Keren et al., 2009) and At.MSP1 were fused in-frame to GFP, introduced into *Arabidopsis* cells, via root

transformation in tissue culture, and analyzed by confocal microscopy (Fig. 1B). As anticipated, the RbcS-GFP showed a typical root plastidial-like fluorescent patterns, whereas the signals of MSP1-GFP were detected as round or rod-shaped particles of about 1 to 2 μm in size, which overlapped with that of the MitoTracker marker, further demonstrating mitochondrial localization of At.MSP1.

MSP1 roles are essential during early embryo-development in *Arabidopsis*

We sought to define the molecular functions of MSP1 by analyzing loss-of-function mutations within the *MSP1* locus. T-DNA insertional-lines inside *MSP1*'s gene-locus available at 'The *Arabidopsis* Information Resource' (TAIR), included SALK-018927 (T-DNA reported to be inserted in the 5' UTR, 192 nucleotides before the start codon), SALK-142675 (*msp1-1*) (T-DNA insertion 312 nucleotides after the start codon), and SALK-070654 (T-DNA reported to be inserted in the 3' UTR, 232 nucleotides after the termination codon) (Figs. 1A, S3A). Sequencing of genomic PCR products spanning the T-DNA insertional junctions confirmed the integrity of the *msp1-1* mutant line (Fig. S3B), but could not support insertional events within the UTRs in the SALK-018927 or SALK -070654 lines.

Similarly to various *emb* mutants (Meinke, 2020), the selfed progeny of the *msp1-1* showed a heterozygous to wild-type segregation ratio of ~2:1 (*i.e.*, 119 out of 175 seedlings). No homozygous seedlings for the *msp1-1* mutant-allele could be recovered among the seeds obtained from the heterozygous plants. Microscopic analyses showed that a quarter of the seeds analyzed in mature-green siliques of *msp1-1* (*i.e.*, 25.1 ± 4.3%, n = 278) were small and deformed, and either collapsed during their development (Fig. 1C-1), or degenerated into shrunken seeds (Fig. 1C-2). A similar seed-morphology, known as *wrinkled1*, was previously associated with altered endosperm metabolism (Focks and Benning, 1998), but is also apparent in various mutants affected in mitochondrial biogenesis (Colas des Francs-Small and Small, 2014). Likewise, the siliques (12~14 days post-fertilization, dpf) of heterozygous *msp1-1* contained ~25% translucent seeds, which contained embryos arrested at the heart-to-torpedo transition stage, whereas their green seeds contained mature embryos (Fig. 1D). As the heterozygous *msp1-1* seedlings were phenotypically indistinguishable from the wild-type plants, we concluded that the insertional event in *MSP1* results in a recessive embryo-arrested phenotype, and that a single copy of the gene is sufficient to support 'normal' embryogenesis and seedling development.

A modified method for embryo-rescue of *Arabidopsis msp1-1* mutant plants

As loss-of-function of *msp1-1* resulted in seed-abortion, we employed a modified embryo-rescue method that was previously used for the recovery of viable homozygous *nmat3* seedlings (Shevtsov-Tal et al., 2021). White seeds collected from surface-sterilized siliques (12~14 dpf) of *msp1-1*, were germinated on MS-agar plates, supplemented with 1% sucrose and vitamins (Fig. 1E). Under these conditions we were able to obtain a few homozygous *msp1-1* plantlets that slowly developed (4-to-5 months) into a six-true-leaf (L6) growth-stage (Boyes et al., 2001). As the *nmat3* mutants, the homozygous *msp1-1* plantlets were able to develop beyond the L6-phase upon their transplant to a liquid growth medium (Fig. 1F). Wild-type embryos collected at the heart-to-torpedo stage (Col-0-heart) achieved a more robust growth than the *msp1-1* mutants (Fig. 1G). We also noticed a phenotypic variation, where some of the *msp1-1* mutants showed a bushy leaf morphology (Fig. 1H), which was also reported for other rescued seedlings, such as *emb* (Franzmann et al., 1989), *ndufv1* (Kuhn et al., 2015), *cod1* (Dahan *et al.*, 2014) or *nmat3* mutants. A small number of rescued *msp1-1* plantlets, which were able to survive when transferred into a potting mix (Fig. 1I), displayed a curled-leaf phenotype (Katz et al., 2004) that was also noted in various *Arabidopsis* mitochondrial mutants (Colas des Francs-Small and Small, 2014). None of the rescued *msp1-1* seedlings was able to flower or to produce seeds. Thus, for the molecular characterization of *msp1*, we used 4~5-month-old embryo-rescued MS-grown plantlets obtained from white seeds of heterozygous *msp1-1*plants. The seedlings were verified to be homozygous by sequencing of genomic PCR products.

Rescuing *msp1-1* phenotypes by a constitutive expression of MSP1

As T-DNA lines often show multiple insertions (O'Malley et al., 2015; Pucker et al., 2021), and since we had only a single mutant line, it was important to confirm that the phenotypes associated with *msp1-1* indeed relate to the loss of MSP1. To facilitate a functional complementation, we cloned the *At.MSP1* gene under the control of 35S-promoter, transformed the construct into heterozygous *msp1-1* mutants and screened for homozygous *msp1-1* plants that harbor the *35S-MSP1* construct. Several plant-lines recovered among the progeny of the T2 plants that contained the *35S:MSP1* transgene, were also homozygous plants for the *msp1-1* insertion (Fig. S3C,

msp1:*35S-MSP1*). One of the lines, plant-18 (Fig. S3C), was included as a control in the subsequent analyses.

msp1 mutants show altered _nad1_ RNA processing in _Arabidopsis_ mitochondria

The mitogenome of *Arabidopsis* harbors 57 genes encoding for different rRNAs, tRNAs and organellar proteins (Sloan et al., 2018; Unseld et al., 1997). We anticipated that MSP1 would function in mtRNA metabolism. At first, the mtRNA profiles of embryo-rescued *msp1-1*, Col-0-heart, heterozygous *msp1-1* complemented *msp1*:*35S-MSP1* and 3-week-old MS-grown Col-0 plants (used as control) were assessed by RT-qPCR with oligonucleotides designed to the different exon-exon and exon-intron regions of each organellar transcript (Table S2). A strong reduction (~10,000-fold) in the steady-state level of transcripts corresponding to a spliced *nad1* exons a-b product was noted in *msp1-1*, as compared to the control 3-week-old Col-0 plants (Fig. 2).

The mitochondrial *nad1*, *nad2*, *nad4*, *nad5*, *nad7*, *cox2*, *ccmFc*, *rpl2* and *rps3* genes are interrupted by group II introns that are removed post-transcriptionally to generate functional/translatable mRNAs. The processing of the *nad1*, *nad2* and *nad5* pre-mRNAs further involves the joining of several exons found in individually expressed gene-fragments, which are physically separated in the mitogenome by *trans*-splicing (Bonen, 2008). The 'breaks' between these gene-fragments are all within the 4th domain (D4) of the *trans*-spliced introns. The maturation of *nad1* involves the processing of three RNA-fragments, *nad1.1*, *nad1.2* and *nad1.3* (Fig. S4A). Two of the *nad1* introns, including the 2nd intron in *nad1.2* (*nad1i477*) and the 4th intron (*nad1i728*) in *nad1.3* are postulated to undergo *cis*-splicing prior to the three RNAs being joined together via the *trans*-splicing of introns 1 (*nad1i394*) and 3 (*nad1i669*) (Bonen, 2008; Brown *et al.*, 2014). Likewise, *nad2* maturation involves the joining of two pre-mRNA fragments separated by intron 2, while *nad5* is fragmented into three gene-pieces within its 2nd and 3rd introns (Bonen, 2008).

Altered splicing is assumed to be present in cases where the accumulation of a specific pre-RNA transcript is correlated with reduced levels of its corresponding mRNA. We considered that the large reduction we observed in transcripts corresponding to spliced *nad1* exons a-b relate to a defect in the excision of the first intron. Yet, the RT-qPCR data indicated that the *nad1.1* pre-RNA (amplified by primers designed to exon 'a' and *nad1* 11) was also notably reduced (about 750-fold) in *msp1-1* mutant. These data indicate to reduced stability of *nad1.1* rather than to altered *nad1* i1 splicing. The moderately increased level (*i.e.*, 5.6 ± 1.2-fold) of *nad1.2* pre-RNA in *msp1-*

1 (amplified by primers designed to the intron's D5 and exon-b) (Fig. 2) is thus anticipated to result as a consequence of the absence of the corresponding *nad1.1* RNA-fragment.

A milder effect was also apparent for *nad2* exons a-b splicing in *msp1-1* (*nad2ab*, 11.2 ± 1.4-fold reduction), while the relative level of the *nad2* i1 pre-RNA was slightly increased (1.5 ± 1.4-fold) in the mutant (Fig. 2). However, we noticed that the splicing efficiencies of *nad2* i1 are also reduced in other *Arabidopsis* mutants affected in the mtRNA metabolism, some of which showing altered *nad1* processing (Table S3). Although various P-class PPRs have been previously shown to affect the splicing of organellar introns (Table S3), our data could not support a direct role for MSP1 in the excision of either *nad1* i1 or *nad2* i1. Other than the effects seen in the processing of *nad1* or *nad2*, the expression of different mtRNAs were seemingly not affected by the loss of MSP1. These included the intron-containing transcripts of *ccmFc*, *cox2*, *nad4*, *nad5*, *nad7*, *rpl2* and *rps3*, as well as the 'intronless' transcripts of *cox1* and *cox3* of CIV, ATP-synthase (CV) subunits, CCM-factors and ribosomal-related genes (Fig. 2). The accumulation of mtRNAs in heterozygous *msp1-1* were generally equivalent to those of the Col-0 plants, while the steady-state levels of many mtRNAs in germinated Col-0-heart embryos were slightly increased (2~4-fold) in comparison to the wild-type plants (Fig. 2). Based on these data, we concluded that the *nad1* processing defects were due to the *msp1* mutation and not the embryo-rescue procedure. Furthermore, the RNA defects seen in *msp1-1* were mostly restored in the 'complemented' line, which express an intact *MSP1* gene (Fig. 2).

***msp1-1* show reduced stability of the *nad1.1* pre-RNA fragment**

We expect that reduced levels of the pre-*nad1.1* transcript and its corresponding spliced *nad1ab* product, rely on altered processing of *nad1.1* pre-RNA, which was not directly assayed in the RT-PCR experiment. This purpose, the mtRNA landscapes in Col-0 and *msp1-1* plants were further examined by RNA-seq analyses, using total seedling RNAs. The transcriptomic data showed that the relative levels of reads corresponding to the *nad1.1* gene-fragment (nucleotides 81,785–83,966), were reduced to residual levels in *msp1-1* (Figs. 3, S4). Analysis of the relative read coverage of each individual exon, between wild-type (Col-0) and *msp1-1* plants, indicated a large reduction in *nad1* exon-a (Fig. 3A). Likewise, the ratio of read coverage between Col-0 and *msp1-1* across the whole *Arabidopsis* mitogenome indicated a single major peak corresponding to the *nad1* exon-a sequence (Fig. 3B). In agreement with the RT-qPCR data, no significant variations

in the maturation of *nad1* exons b-c, c-d, or d-e transcripts were evident in the RNA-seq data (Figs. 3, S4). A minor increase in nucleotide abundances in *msp1-1* was apparent for *nad2* i1 (Data S1), whereas the levels and read-depth profiles of *nad2-a*, *nad2-b*, or other mtRNA transcripts in *msp1-1* were mostly equivalent to those of the wild-type plants (Figs. 3, S4, Data S1). Taken together, these data showed that MSP1 has a key role in the stabilization of *nad1.1* pre-mRNA, and that the loss of MSP1 reduces the excision efficiency of *nad2* i1, an effect which may relate to altered mitochondria biogenesis and/or gene-expression (Table S3).

MSP1 is expected to be associated with an RNA motif found in its defined intron target

A combinatorial code for RNA-recognition by PPR proteins has been worked out, where amino acids at positions 5 and 35 of each domain act as specificity-determining residues (Barkan *et al.*, 2012; Cheng et al., 2016). Several PPRs were previously shown to affect the stability of their RNA-ligands by protecting them from excessive exonuclease activities (Barkan and Small, 2014). *In-silico* data (see Fig. S5A) indicate the preferred sequence 5'-UACCAAAAGGU for MSP1's PPR 4-11 motifs, while PPRmatcher (Royan et al., 2021) was used to score potential alignments to every possible position (735,616x) in the mtDNA (Fig. S5B). Comparative analyses with the updated *Arabidopsis* mitogenome (Sloan *et al.*, 2018), revealed three mtDNA loci exactly matching this sequence. One of these is found within the *nad1* i1, 1,140 bp downstream to exon-a (nucleotides 81,785-81,796) (Figs. 3A, S4A, S5), whereas the two other sites are mapped to noncoding/unexpressed loci. The RNA-seq data of Col-0 plants showed that the relative read-depth in the *nad1.1* region is noticeably reduced immediately following the predicted MSP1 binding-site (Fig. 3C). These data strongly support the association of MSP1 with a specific region in D4 of *nad1* i1, which may be required for the correct 3'-end processing of *nad1.1* transcript.

MSP1 binds to *nad1.1* by associating with nucleotides at the predicted binding site and protects *nad1* i1 from excessive 3'-to-5' exonucleolytic degradation, *in-vitro*

The binding activity and specificity of MSP1 to *nad1.1* RNA was analyzed by biochemical analyses, in vitro. As attempts to express and purify an intact MSP1 were unsuccessful, we analyzed the binding properties of a recombinant product, which harbors the PPR motifs 4-14 of MSP1. The codon optimized rMSP1 construct was cloned in-frame to GST in its N-terminus and a C-terminal 6xHis tag, expressed in *E. coli*, purified by affinity chromatography (Fig. S6), and

studied for its binding characteristics by filter-binding assays (Keren et al., 2008). The rMSP1 protein was found to binds to *nad1* i1 (nucleotides 80,646-81,796) with a micromolar affinity (calculated $K_d = 4.01 \pm 0.31$ μM) and binding stoichiometry (n) of 1.0 ± 0.05 (Fig. 4A). We further analyzed the association between rMSP1 and a *nad1* i1 RNA-ligand (i.e., *nad1.1*-ΔMBS) that is lacking the postulated MSP1 binding site (MBS, UACCAAAAGGU). The binding activity of rMSP1 to *nad1.1*-ΔMBS was found to be notably lower ($K_d = 37.06 \pm 7.93$ μM) than that of the 'intact' *nad1* i1. For binding competition experiments, a synthetic UACCAAAAGGU RNA-oligo was used in the binding reactions in a 100:1 molar ratio to *nad1* i1. In support of the specific association of MSP1 with this region, the addition of the competitor RNA reduced the maximal amount of bound *nad1* i1 by about 3 orders of magnitude ($K_d \approx 13$ mM), whereas the binding of MSP1 to *nad1* i1 was seemingly unaffected by a synthetic poly-C RNA-oligo (Fig. 4B, $K_d = 3.77 \pm 0.39$ μM). No binding activity was indicated for GST alone, which was used as a control for the integrity of the binding assays.

Here, we further aimed to determine whether the binding of MSP1 to the UACCAAAAGG site may relate to the altered *nad1.1* stability seen in *msp1-1* mutant. PNPase-protection assays with 5'-labeled *nad1* i1 RNA-ligands, further indicated a role for MSP1 as a mitochondrial *nad1.1* stability factor. The addition of rMSP1 to the reaction assays led to the accumulation of a specific RNA product of ~100 nts, generated by the 3'-to-5' PNPase exonuclease (Figs. 3A, S4A), which is expected to corresponds to the mature *nad1.1* transcript seen in the RNA-seq data. Notably, the trimmed RNA was generated by the PNPase with two different RNA templates with the same 5'-regions upstream to the MBS, but harbored 30- or 300-nts intronic tails downstream to the MBS. In the absence of rMSP1, the *nad1.1* RNA ligand was fully digested by the PNPase (Fig. 4B). Likewise, the rMSP1 was not able to protect the *nad1.1*-ΔMBS transcript, which is lacking the UACCAAAAGGU site, from exonucleolytic processing by PNPase (Fig. 4B). rMSP1 also failed to stabilizes *nad1* i1 from endonucleolytic cleavage by the Benzonase enzyme. The canonical RNAse A enzyme worked like Benzonase, and also led to the complete degradation of *nad1* i1 in the presence or absence of rMSP1 (Fig. 4B).

MSP1 functions are required for the biogenesis of respiratory CI in *Arabidopsis* plants

Nad1 is essential for CI biogenesis and function (Braun et al., 2014; Guerrero-Castillo et al., 2017; Ligas et al., 2019). The RNA maturation defects we see (Figs. 2-3, S4-S5) suggest that Nad1 exists

in extremely low levels (or absent) in the mutant-line. Altered *nad2* maturation is also anticipated to affect the biogenesis of the respiratory system, as Nad2 is also postulated to be incorporated during initial stages in CI assembly in Arabidopsis plants (Ligas *et al.*, 2019). The relative accumulation of different organellar proteins in *msp1-1* versus Col-0 plants was estimated by immunoblotting. These analyses indicated that Nad1 (~36 kDa) (Shevtsov-Tal *et al.*, 2021) is reduced to trace levels in *msp1-1*, but is clearly visible in the heterozygous, Col-0-heart or 'complemented' lines (Fig. 5A, Table S5A). The appearance of various bands in the Nad1-blot of *msp1-1* may correspond to aberrant Nad1 products that can be translated by alternative AUG sites present in semi-processed *nad1* transcripts (Figs. 2-3), which are recognized by the polyclonal anti-Nad1 antibodies. The steady-state levels of CA2 (30 kDa) and Nad9 (23 kDa) subunits of the 'membranous' and 'soluble' domains, respectively, of CI were found to be slightly higher in *msp1-1* than in Col-0 plants (*i.e.*, 3.7 ± 0.5 and 2.1 ± 0.3, respectively). The level of Atp2 (CV) in *msp1-1* was equivalent to that of the Col-0 plants, whereas the signals of the nuclearly-encoded Atp1 (CV), RISP (CIII), VDAC, or the organellar-encoded COX2 (CIV), were found to be higher in the mutant or Col-0-heart seedlings (Fig. S7A, Table S5A). The accumulation of different organellar proteins in heterozygous *msp1-1* was generally equivalent to Col-0 plants.

The respiratory system in plants also possesses type-II NAD(P)H dehydrogenases (NDs) and alternative oxidases (AOXs) (Møller et al., 2021; Popov et al., 2020). In *Arabidopsis*, mutants affected in their respiration typically show notable increases in the expression or accumulation of AOXs and NDs. Likewise, the immunoblots indicated that AOX1/2 signal was higher in the *msp1-1* mutant (Fig. S7A, Table S5A). An upregulation in the accumulation of several AOXs and NDs was also evident by RT-qPCR, where transcripts corresponding to AOX2, NDA2, AOX1A or NDB2 were increased in the mutant by 3.2-, 3.4-, 16- and 10-fold, respectively (Fig. S7B).

Considering the effects of MSP1 on Nad1 expression, we further analyzed the relative abundances of native respiratory complexes I, III, IV and V in Col-0 and mutant plants by Blue-native (BN) PAGE analyses (Figs. 5B, S7C). Arrows indicate native complexes I (~1,000 kDa), CIII dimer (III_2, ~500 kDa), supercomplex I+III_2 (about 1,500 kDa) (Braun *et al.*, 2014; Senkler *et al.*, 2017), CIV (~220 kDa), and CV (~700 kDa). The BN-PAGE/immunoblot analyses showed that CI is below detectable levels in *msp1-1*, but is correctly assembled in the complemented line (Fig. 5B, Table S5B). A significant reduction in CI was also evident by '*in-gel*' CI-activity assays, which further indicated that none of the sub-CI particles in *msp1-1* were active (Fig. 5B). No

significant changes in CI accumulation were seen in the heterozygous line. The immunoblots of CA2 also indicated the presence of CI assembly intermediates (Ligas *et al.*, 2019) of about 170-to-700 kDa in size in *msp1-1* (Fig. 5B-I*). BN-PAGE analyses of *nmat1*, which is impaired in the splicing of *nad1* i1 (Keren et al., 2012), also indicated the presence of sub-CI particles, with a dominant band of ~700 kDa (Fig. S6). Accumulation of partially-assembled CI intermediates was also evident in the germinated embryos of Col-0, but these plants (Col-0-heart) rather exhibited increased CI level and activity (Fig. 7, Table S5B). Due to the cross-reactivity of the anti-Nad1 antibodies with various organellar proteins (Fig. 5B) (Shevtsov-Tal *et al.*, 2021), it was impossible to determine whether the CI intermediates harbor the Nad1 protein.

The BN-PAGEs further showed that CIII, CIV and CV are more abundant in *msp1-1* (possibly to accommodate changes in electron transport and/or H^+-pumping rates following the loss of holo-CI), while their levels in the complemented line were generally equivalent to those of the Col-0 seedlings (Fig. S7C, Table S5B). The loss of CI in the *msp1-1* mutant-line is further correlated with the upregulation of mRNAs and proteins associated with the alternative pathway of the electron transport (*i.e.*, NDs and AOXs) (Figs. S7A, S7B).

Discussion

MSP1 encodes a PPR factor that is pivotal for *nad1* pre-RNAs maturation

MSP1 is a mitochondrion-localized PPR protein (Figs. 1, S2), which has indispensable functions during embryo-development (Table 1, Fig. 1). Embryogenesis and seed-germination are complex developmental processes that rely on increased cellular metabolism to support their high-energy demands (Best *et al.*, 2020a). These correlate with experimental data that show that the expression/processing of mtRNAs in plants are both developmentally and environmentally responsive (Dalby and Bonen, 2013; Law et al., 2012; Li-Pook-Than et al., 2004). Likewise, the expression of different factors that function in mtRNA metabolism, including MSP1 (Fig. S1), seems to be tightly regulated during early plant life or under stress conditions (Chen et al., 2018; Law *et al.*, 2012). To gain more insights into the roles of MSP1, we analyzed an embryo-rescued *msp1-1* knockout-line and complemented plants expressing the *MSP1* gene (Figs. 1, S3, Table S6). Our data show that *msp1* mutants are strongly affected in the maturation of *nad1* exon-a (Figs. 2-3), whose processing involves the splicing of two mtRNA fragments, *nad1.1* and *nad1.2*, separated by intron 1 (Fig. S4A). The analysis of the RNA profiles of Col-0 and *msp1* plants indicated that

MSP1 has a key role in *nad1.1* transcript maturation, by a molecular mechanism that is not directly related with the splicing of *nad1* i1 (i.e., splicing defects are typically associated with the accumulation of pre-RNAs and the reduced levels of their corresponding mRNAs).

Various PPRs have been implicated in the post-transcriptional generation of 5' or 3' termini of organellar transcripts in plants (Barkan and Small, 2014). In *Arabidopsis* mitochondria, these include at least MTSF1, MTSF2, PPR19, RPF1, RPF2, RPF3, MTSF3 (Colas des Francs-Small and Small, 2014; Wang et al., 2022; Zmudjak and Ostersetzer-Biran, 2017). These may drive the accumulation of short RNA footprints (cosRNAs), often corresponding to the precise termini of organellar transcripts (Pfalz et al., 2009; Ruwe and Schmitz-Linneweber, 2012). Likewise, the MSP1 binding site is located at the very end of the mature *nad1.1* transcript (Figs. 3C, S4, S5), although was not previously identified among the mitochondrial cosRNAs (these are seemingly less obvious than the plastidial ones) (Ruwe et al., 2016). The RNA-seq data (Figs. 4, S4, S5) further showed that *nad1.1* is reduced to residual levels in the *msp1* mutant, indicating that MSP1 is pivotal for its accumulation. Based on these data we speculated that through its association with a specific site in *nad1.1* (Fig. 4, S4A, S5), MSP1 facilitates the generation of its 3'-terminus and stabilizes it - a prerequisite for the *trans*-splicing of *nad1* i1. In-vitro biochemical assays provided with further evidence that the association of MSP1 with *nad1.1* rely on the UACCAAAAGGU site (Fig. 4A), and that this interaction is sufficient to block 3′→5′ degradation by the PNPase beyond this site, but not to protect the RNA from endonucleolytic digestion (Fig. 4B).

The excision of *nad2* i1 in angiosperms: an epistatic regulation associated with mtRNA metabolism or the biogenesis status of the OXPHOS system?

A specific role for MSP1 in the excision of *nad2* i1 remains ambiguous. A region with a limited homology to the predicted MSP1 binding site can be found in *nad2* i1 (CAAAAGGU, nts 162,555-162,562). It is possible, therefore, that MSP1 may enhance the excision efficiency of *nad2* exons a-b, *e.g.*, by assisting in the folding of this highly-derived intron-RNA (Bonen, 2008). However, reduced *nad2* i1 splicing is also evident in many other mutants affected in mtRNA metabolism (Table S3). It is possible that the processing of various mtRNAs (e.g., *nad1*, *nad5*, or *nad7*) is linked to the splicing of *nad2* i1 through an as yet unknown mechanism. Alternatively, the altered processing of *nad2* may involve an epistatic effect (for example, the translation rates of some mRNAs in algae chloroplasts are orchestrated with the *de-novo* assembly of their related

complexes) (Choquet and Wollman, 2009). Unassembled CI subunits may thus interfere with the processing of *nad2* i1However, the excision of *nad2* i1 was not affected in *ca2* mutant (Fig. S8)(Cordoba et al., 2016), while only a minor reduction in *nad2* levels was evident in a mutant missing the 18-kD subunit of CI and is also strongly affected in CI assembly (Meyer et al., 2009). Based on these data, it is unlikely that CI biogenesis can be directly or indirectly related to *nad2* pre-RNA processing. Other than the processing defects seen in *nad1* and *nad2,* the expression of other organellar transcripts remained mostly intact in *msp1-1* (Figs. 2-3, Data S1).

The evolution of a *nad1ab trans*-splicing event in the mitochondria of spermatophytes

The regions corresponding to the first two exons in *nad1* in the mitogenomes of algae or basal land plants, such as liverworts (as their bacterial *NuoH*-related genes), are found as uninterrupted 'intronless' reading-frames. The *nad1* i1 (*nad1i394*) sequence is also not present in the mtDNAs of mosses, or hornworts, which harbor another intron (*nad1i287*) in a different mtDNA-locus (Fig. 6). Within angiosperms (besides *Viscum* sp. that lacks the *nad* genes entirely, (Petersen et al., 2015; Skippington et al., 2015), contain a *trans*-spliced *nad1* i1 where the putative MSP1 binding site seems perfectly conserved (Figs. 6, S9). Comparative analyses of genomic plant databases indicated that genes related to *MSP1* are present in both monocot and dicot species (Figs. 6, S10A). Particularly, the homologous gene in maize (*DEK2*) (Fig. S10B) was shown to affect the processing of *nad1* (Qi et al., 2017). Based on RT-PCRs, the authors considered a role for DEK2 in the splicing of *nad1* i1 (Qi *et al.*, 2017). Yet, the accumulation of *nad1.1* was not assessed, and thus it is possible, even likely, that DEK2 has a similar role to that of MSP1, *i.e.*, the stabilization of *nad1.1* transcript. The predicted RNA-binding site for DEK2 is identical to that of MSP1 (Fig. S9), and is present in the equivalent position at the end of the *nad1.1* (nts. 120612-120603) in the mtDNA of maize (NC_007982). We further noted that the transformation of the *Zm.DEK2* gene into Arabidopsis, complements the *msp1* mutation and restores the maturation of *nad1ab* (Fig. 2), demonstrating that *DEK2* encodes an orthologue of Arabidopsis.

We anticipated that gymnosperms also encode homologs of the MSP1/DEK2 proteins. Yet, no potential orthologs for these factors could be supported in gymnosperms, although the intronic binding site is perfectly conserved in these plants (Fig. S9). It is therefore anticipated that this site has already been under selection in early spermatophytes, apparently as a target for a different (PPR) factor. Still, an orthologues MSP1 factor might be identified in some gymnosperms, once

full genome assemblies are established for different cycads, ginkgo, yews or conifers (Liu et al., 2021). Based on these observations, we speculate that MSP1 was recruited about 150~200 MYA (Delwiche and Cooper, 2015; Kenrick et al., 2012), possibly through a genomic gene-duplication event, to facilitate the generation of 3'-ends in fragmented *nad1* i1 sequences present in the mtDNAs of early spermatophytes. The ability of different intron-RNA segments to splice in *trans* could be followed by genome fragmentation, *i.e.*, recombination and insertion of individual transcriptional initiation and termination sites during evolution. In fact, *trans*-splicing can be facilitated in model group II introns that are artificially fragmented in D4 (Belhocine et al., 2008). This remarkable molecular mechanism seems related to the evolution of the spliceosomal system (Schmitz-Linneweber *et al.*, 2015; Zimmerly and Semper, 2015). An important question that remains is whether MSP1 is also involved in other activities, *e.g.*, the recruitment of splicing cofactors, or in the association between the *nad1.1* and *nad1.2* fragments to form a catalytically active intron-RNP complex. In regard to these functions, the EMB2654 and PPR4 proteins are required for the *trans*-splicing of the plastidial *rps12* transcripts and not for transcript accumulation, even though they bind near the ends of their respective transcripts (Lee et al., 2019). These data indicate that RNA stabilization and splicing are not necessarily linked to one another, but such effects cannot be ruled out, at this time, for the mitochondrial MSP1 in Arabidopsis.

Impaired CI biogenesis in *msp1* mutants and its effect on embryogenesis, seed-germination and plant development

The *nad1* and *nad2* processing defects we observed in *msp1* result in altered biogenesis of the OXPHOS system. The respiratory machinery is made of four major electron transport carriers, denoted as CI-to-CIV, and the ATP synthase enzyme (CV). BN-PAGE followed by immunoblot and '*in-gel*' activity assays indicated that a holo-CI cannot be assembled in *msp1* mutants, which lack the Nad1 protein (Figs. 5), whereas the levels of the respiratory complexes CIII, CIV and CV were increased in the mutant (Fig. S7, Table S5). The higher accumulation of other respiratory complexes is anticipated to be associated with the need to increase ATP production due to loss of CI, as well as for the homeostasis of reduced NADH, whose accumulation can be toxic to the cell (Yang et al., 2020). The defects in CI biogenesis are likely to be associated with respiration through different NDs and AOXs, which are upregulated in mitochondrial mutants, as well as in *msp1* (Fig. S4B). The molecular basis for the phenotypic variation in development and respiration between

different mutants remains unclear, and may relate to residual differences in CI levels (Kuhn *et al.*, 2015), or to development effects mediated by retrograde (mitochondrial-to-nuclear) signaling pathways (Schwarzländer *et al.*, 2012; Woodson and Chory, 2008).

Nad1 is proposed to be incorporated early during CI biogenesis, and was previously identified mainly in a ~450 kDa sub-CI particle by MS-MS analysis of CI mutant lines (Ligas *et al.*, 2019). The BN-PAGE indicated the presence of partially assembled CI intermediates in both *msp1* and *nmat1* mutants (with a major band of ~700 kDa) (Figs. 5B, S7). Based on the BN-PAGE data, Nad1 may be incorporated at more advanced stages during CI assembly (after or together with Nad4 or Nad5 subunits) (Ligas *et al.*, 2019), as was proposed for the CI assembly pathway in bacteria (Friedrich et al., 2016). The differences seen in patterns of sub-CI particles in the different mutant-lines likely correspond to different levels of *nad1* mRNA between, i.e., *nmat1* (reduced levels) (Keren *et al.*, 2012) and *msp1* (below detectable levels, Figs. 2-4, S4).

A loss of MSP1 function is detrimental during early embryogenesis, most likely as the Nad1 protein is essential for the biogenesis of an active holo-CI (Braun *et al.*, 2014; Ostersetzer-Biran, 2016) (Fig. 5B, S7C). Likewise, the germination of *msp1-1* seeds was enabled only under in-vitro conditions (Shevtsov-Tal *et al.*, 2021) (Fig. 1C). These were able to continue their development beyond the L6 growth stage only when transferred to a liquid MS medium. Why does the loss of MSP1 or nMAT3 (Shevtsov-Tal *et al.*, 2021), cause a major embryo-defect, while the seeds of *nmat1*, *nmat4*, *otp43*, and other mutants with altered processing of *nad1* i1 and CI biogenesis defects (Colas des Francs-Small and Small, 2014), seem to be able to complete the embryonic development? We speculate that the variations in growth and development also relate to Nad1 levels. While *nmat1*, *nmat4* or *otp43* accumulate basal levels of Nad1, the protein is likely absent, or at levels below a critical threshold to promote CI functions, in *msp1* or *nmat3* plants.

Methods

Plant material and growth conditions

Arabidopsis thaliana (ecotype Columbia-0) was used in all experiments. Wild-type (Col-0) and *mps1* mutant line SALK-142675 (*msp1-1*), SALK-018927 and SALK-070654 were obtained from ABRC, at Ohio State University. The growth conditions used for the analysis of wild-type and mutant lines were identical to those described previously (Shevtsov-Tal *et al.*, 2021).

GFP localization assays

The N-terminal region (300 bps) of *MSP1* (*AT4G20090*) gene was fused in-frame to GFP coding sequence and cloned into a modified pCAMBIA binary vector (gift of Dr. Yoram Eyal, ARO). *In-vivo* protein localization by GFP fusion were performed via root transformation in tissue culture, similarly to the method described by Weigel and Glazebrook (2006).

Embryo rescue and establishment of homozygous *MSP1* mutants

The development of *msp1* mutant-line embryos was performed essentially as described previously (Shevtsov-Tal *et al.*, 2021), using white seeds obtained from green mature siliques of wild-type or heterozygous *msp1-1* (SALK-line 142675) plants.

Plant transformation and functional complementation of the *MSP1-1* mutation

A 1,989 bp fragment containing the coding region of *MSP1* was generated by PCR, cloned under the control of the 35S promoter region within pCAMBIA-2300 vector, and used to transform *msp1-1* plants by a floral-dip method.

Microscopic and macroscopic analyses of *Arabidopsis* wild-type and mutant plants

Analysis of whole plant morphology, roots, leaves, siliques and seeds of wild-type and mutant lines were examined under a stereoscopic (dissecting) microscope or light microscope at the Bio-Imaging unit of the Institute of Life Sciences (The Hebrew University of Jerusalem, Israel).

RNA extraction and analysis

RNA extraction and analysis were performed essentially as described previously (Shevtsov-Tal *et al.*, 2021; Sultan et al., 2016).

Transcriptome mapping by high-throughput (RNA-seq) analysis

Total plant RNA was extracted from *Arabidopsis* wild-type and mutant lines. Sequencing was carried out by IDT (Synthezza, Jerusalem, Israel) with HTS-Illumina platform, used for a paired-end 150-bp sequencing strategy.

Preparation of recombinant MSP1 protein

A g-Block fragment (Synthezza, Jerusalem, Israel) containing the MSP1s' PPRs 4-14 motifs was cloned into pGEX-4T1, in-frame to GST in its N-terminus and a C-terminal 6xHis tag. The recombinant protein (rMSP1) was expressed in *E. coli*, and purified by affinity chromatography.

In-vitro RNA binding assays

Filter-binding assays were performed with a slot-blot manifold, essentially as described previously (Keren *et al.*, 2008; Ostersetzer et al., 2005). The fraction of bound RNA was calculated as the ratio between the signal of the RNA captured by the protein and total RNA signals (protein-bound and free RNAs).

Exonuclease and endonuclease protection assays

PNPase protection assays were perform essentially as described by Prikryl et al. (2011). ^{32}P-labeled RNAs were denatured and snap cooled on ice, before was used in the reaction assays, using rMSP1, PNPase, Benzonase or RNase A. The samples were denatured by heating in 60% formamide sample buffer and resolved on 10% AA/7M urea gels, in 1×TBE buffer.

Enriched mitochondrial membrane preparation and analysis

BN-PAGE was performed according to the method described previously (Pineau et al., 2008). An aliquot equivalent to 40 mg tissue was solubilized with 5% (w/v) digitonin in BN-solubilization buffer and loaded onto a native 4-16% linear gradient gel. For immunoblotting, the gel was transferred to a PVDF membrane. CI activity assays were performed essentially as described previously (Eubel et al., 2005).

Data availability

High-throughput RNA sequences are available as BioProjects PRJNA704631 and PRJNA768306. Genome Maps is an opensource collaborative initiative available in the GitHub repository (https://github.com/compbio-bigdata-viz/genome-maps). A complete version of the Materials and Methods is available in the supplemental information.

Acknowledgments

We thank Dr. Etienne Meyer for providing the anti-NAD1 antibodies, Prof. Hans-Peter Braun for providing us laboratory procedures for BN-PAGE analysis, Prof. Ariel Chipman for his help with Nomarski microscopy analyses, and Dr. Hakim Mireau for his help with MSP1 binding predictions and useful discussions regarding the role of MSP1 in mtRNA metabolism. A very special thank goes to Dr. Michal Zmudjak, a former graduate student of O.O.B, for her inspiring role in establishing the modified embryo-rescue method.

Author contributions

Dr. Corinne Best: Plant growth and analysis, establishment of embryo rescued mutant lines, RNA and protein analysis. Ron Mizrahi: Expression and analysis of recombinant MSP1 protein and its RNA binding characteristics, help with GFP localization analysis. Rana Edris: Plant growth and analysis of *ca2* mutant lines. Hui Tang: Phylogenetic analysis of the MSP1 protein family. Dr. Hagit Zer: GFP localization analysis, cloning, assisted in the expression of recombinant proteins. Dr. Catherine Colas des Francs-Small: analysis of the RNA landscapes of wild type and mutant lines. Dr. Omri M. Finkel: assisted with Bioinformatic analyses of the RNA landscapes of wild-type plants and mutant lines. Prof. Hongliang Zhu: Bioinformatic analyses, phylogenetic map of the MSP1 protein family in plants. Prof. Ian Small: analysis of the RNA landscapes of wild type and mutant lines, prediction of MSP1 RNA binding site, and manuscript preparation. Prof. Oren Ostersetzer-Biran: PI, manuscript preparation and corresponding author.

Funding

This work was supported by grants to O.O.B from the 'Israeli Science Foundation' ISF grants no. 1834/20 and 3254/20, and by grants to H.Z. from the National Natural Science Foundation of China (32061143022).

Conflict of interest

The authors confirm that they have no conflict of interest to declare.

References

Barkan, A., and Small, I. (2014). Pentatricopeptide repeat proteins in plants. Annu Rev Plant Biol **65**:415-442. doi:10.1146/annurev-arplant-050213-040159.

Barkan, A., Klipcan, L., Ostersetzer, O., Kawamura, T., Asakura, Y., and Watkins, K.P. (2007). The CRM domain: An RNA binding module derived from an ancient ribosome-associated protein. RNA **13**:55-64. 10.1261/rna.139607.

Barkan, A., Rojas, M., Fujii, S., Yap, A., Chong, Y., Bond, C., and Small, I. (2012). A combinatorial amino acid code for RNA recognition by pentatricopeptide repeat proteins. PLoS Genet **8**:e1002910.

Belhocine, K., Mak, A.B., and Cousineau, B. (2008). Trans-splicing versatility of the *Ll.LtrB* group II intron. RNA **14**:1782-1790. 10.1261/rna.1083508.

Berardini, T.Z., Reiser, L., Li, D., Mezheritsky, Y., Muller, R., Strait, E., and Huala, E. (2015). The Arabidopsis information resource: Making and mining the "gold standard" annotated reference plant genome. Genesis **53**:474-485. https://doi.org/10.1002/dvg.22877.

Best, C., Mizrahi, R., and Ostersetzer-Biran, O. (2020a). Why so complex? The intricacy of genome structure and gene expression, associated with angiosperm mitochondria, may relate to the regulation of embryo quiescence or dormancy-intrinsic blocks to early plant life. Plants **9**:1-19. 10.3390/plants9050598.

Best, C., Sultan, L., Murik, O., and Ostersetzer-Biran, O. (2020b). Insights into the mitochondrial transcriptome landscapes of two Brassicales plant species, *Arabidopsis thaliana* (var. Col-0) and *Brassica oleracea* (var. botrytis). Endocytobiosis Cell Res **30**:16-38.

Bonen, L. (2008). Cis- and trans-splicing of group II introns in plant mitochondria. Mitochondrion **8**:26-34. DOI: 10.1016/j.mito.2007.09.005.

Boyes, D.C., Zayed, A.M., Ascenzi, R., McCaskill, A.J., Hoffman, N.E., Davis, K.R., and Görlach, J. (2001). Growth stage–based phenotypic analysis of Arabidopsis. A model for high throughput functional genomics in plants. Plant cell **13**:1499-1510. 10.1105/tpc.010011.

Braun, H.-P., Binder, S., Brennicke, A., Eubel, H., Fernie, A.R., Finkemeier, I., Klodmann, J., König, A.-C., Kühn, K., Meyer, E., et al. (2014). The life of plant mitochondrial complex I. Mitochondrion **19**:295-313. http://dx.doi.org/10.1016/j.mito.2014.02.006.

Brown, G.G., Colas des Francs-Small, C., and Ostersetzer-Biran, O. (2014). Group II intron splicing factors in plant mitochondria. Frontiers Plant Sci **5**:1-13. 10.3389/fpls.2014.00035.

Cai, M., Li, S., Sun, F., Sun, Q., Zhao, H., Ren, X., Zhao, Y., Tan, B.C., Zhang, Z., and Qiu, F. (2017). Emp10 encodes a mitochondrial PPR protein that affects the *cis*-splicing of *nad2* intron 1 and seed development in maize. Plant J **91**:132-144. 10.1111/tpj.13551.

Candales, M.A., Duong, A., Hood, K.S., Li, T., Neufeld, R.A.E., Sun, R., McNeil, B.A., Wu, L., Jarding, A.M., and Zimmerly, S. (2011). Database for bacterial group II introns. Nucleic Acids Res **40**:187-190. 10.1093/nar/gkr1043.

Chen, G., Zou, Y., Hu, J., and Ding, Y. (2018). Genome-wide analysis of the rice PPR gene family and their expression profiles under different stress treatments. BMC Genomics **19**:720. 10.1186/s12864-018-5088-9.

Cheng, S., Gutmann, B., Zhong, X., Ye, Y., Fisher, M.F., Bai, F., Castleden, I., Song, Y., Song, B., Huang, J., et al. (2016). Redefining the structural motifs that determine RNA binding and RNA editing by pentatricopeptide repeat proteins in land plants. Plant J **85**:532-547. 10.1111/tpj.13121.

Choquet, Y., and Wollman, F.-A. (2009). Chapter 29 - The CES Process. In The Chlamydomonas Sourcebook (Second Edition), E.H. Harris and D.B. Stern and G.B. Witman, eds. (Academic Press: London), pp. 1027-1063. https://doi.org/10.1016/B978-0-12-370873-1.00037-X.

Ci Rdoba, J.P., Fassolari, M., Marchetti, F., Soto, D.B., Pagnussat, G.C., and Zabaleta, E. (2019). Different types domains are present in complex I from immature seeds and of CA adult plants in *Arabidopsis thaliana*. Plant Cell Physiol **60**:986-998. 10.1093/pcp/pcz011.

Cohen, S., Zmudjak, M., Colas des Francs-Small, C., Malik, S., Shaya, F., Keren, I., Belausov, E., Many, Y., Brown, G.G., Small, I., et al. (2014). nMAT4, a maturase factor required for *nad1* pre-mRNA processing and maturation, is essential for holocomplex I biogenesis in Arabidopsis mitochondria. Plant J **78**:253-268. 10.1111/tpj.12466.

Colas des Francs-Small, C., and Small, I. (2014). Surrogate mutants for studying mitochondrially encoded functions. Biochimie **100**:234-242. http://dx.doi.org/10.1016/j.biochi.2013.08.019.

Cordoba, J.P., Marchetti, F., Soto, D., Martin, M.V., Pagnussat, G.C., and Zabaleta, E. (2016). The CA domain of the respiratory complex I is required for normal embryogenesis in *Arabidopsis thaliana*. J Exp Bot **67**:1589-1603. 10.1093/jxb/erv556.

Cushing, D.A., Forsthoefel, N.R., Gestaut, D.R., and Vernon, D.M. (2005). Arabidopsis *emb175* and other *ppr* knockout mutants reveal essential roles for pentatricopeptide repeat (PPR) proteins in plant embryogenesis. Planta **221**:424-436. 10.1007/s00425-004-1452-x.

Dahan, J., Tcherkez, G., Macherel, D., Benamar, A., Belcram, K., Quadrado, M., Arnal, N., and Mireau, H. (2014). Disruption of the *CYTOCHROME C OXIDASE DEFICIENT1* gene leads to cytochrome c oxidase depletion and reorchestrated respiratory metabolism in Arabidopsis. Plant Physiol **166**:1788-1802. 10.1104/pp.114.248526.

Dai, L.X., Toor, N., Olson, R., Keeping, A., and Zimmerly, S. (2003). Database for mobile group II introns. Nucleic Acids Res **31**:424-426.

Dalby, S.J., and Bonen, L. (2013). Impact of low temperature on splicing of atypical group II introns in wheat mitochondria. Mitochondrion **13**:647-655. http://dx.doi.org/10.1016/j.mito.2013.09.001.

Delwiche, C.F., and Cooper, E.D. (2015). The evolutionary origin of a terrestrial flora. Curr Biol **25**:R899-910. 10.1016/j.cub.2015.08.029.

Deng, D., Yan, C., Pan, X., Mahfouz, M., Wang, J., Zhu, J.K., Shi, Y., and Yan, N. (2012). Structural basis for sequence-specific recognition of DNA by TAL effectors. Science **335**:720-723. 10.1126/science.1215670.

Ding, Y.H., Liu, N.Y., Tang, Z.S., Liu, J., and Yang, W.C. (2006). Arabidopsis GLUTAMINE-RICH PROTEIN23 is essential for early embryogenesis and encodes a novel nuclear PPR motif protein that interacts with RNA polymerase II subunit III. Plant Cell **18**:815-830. 10.1105/tpc.105.039495.

Emanuelsson, O., Nielsen, H., Brunak, S., and Heijne, G.v. (2000). Predicting subcellular localization of proteins based on their N-terminal amino acid sequence. J Mol Biol **300**:1005-1016.

Eubel, H., Braun, H.-P., and Millar, A.H. (2005). Blue-native PAGE in plants: a tool in analysis of protein-protein interactions. Plant methods **1**:11-11. 10.1186/1746-4811-1-11.

Falcon de Longevialle, A., Meyer, E.H., Andres, C., Taylor, N.L., Lurin, C., Millar, A.H., and Small, I.D. (2007). The pentatricopeptide repeat gene OTP43 is required for *trans*-splicing of the mitochondrial *nad1* intron 1 in *Arabidopsis thaliana*. Plant Cell **19**:3256-3265. 10.1105/tpc.107.054841.

Focks, N., and Benning, C. (1998). Wrinkled1: A novel, low-seed-oil mutant of Arabidopsis with a deficiency in the seed-specific regulation of carbohydrate metabolism. Plant Physiol **118**:91-101.

Franzmann, L., Patton, D.A., and Meinke, D.W. (1989). In vitro morphogenesis of arrested embryos from lethal mutants of *Arabidopsis thaliana*. Theor Appl Genet **77**:609-616. 10.1007/bf00261231.

Friedrich, T., Dekovic, D.K., and Burschel, S. (2016). Assembly of the Escherichia coli NADH:ubiquinone oxidoreductase (respiratory complex I). BBA - Bioenergetics **1857**:214-223. https://doi.org/10.1016/j.bbabio.2015.12.004.

Fromm, S., Braun, H.P., and Peterhansel, C. (2016a). Mitochondrial gamma carbonic anhydrases are required for complex I assembly and plant reproductive development. New Phytol **211**:194-207. 10.1111/nph.13886.

Fromm, S., Going, J., Lorenz, C., Peterhansel, C., and Braun, H.P. (2016b). Depletion of the "gamma-type carbonic anhydrase-like" subunits of complex I affects central mitochondrial metabolism in *Arabidopsis thaliana*. Biochim Biophys Acta **1857**:60-71. 10.1016/j.bbabio.2015.10.006.

Fuchs, P., Rugen, N., Carrie, C., Elsasser, M., Finkemeier, I., Giese, J., Hildebrandt, T.M., Kuhn, K., Maurino, V.G., Ruberti, C., et al. (2020). Single organelle function and organization as estimated from Arabidopsis mitochondrial proteomics. Plant J **101**:420-441. 10.1111/tpj.14534.

Gobert, A., Gutmann, B., Taschner, A., Gossringer, M., Holzmann, J., Hartmann, R.K., Rossmanith, W., and Giege, P. (2010). A single Arabidopsis organellar protein has RNase P activity. Nat Struct Mol Biol **17**:740-744. 10.1038/nsmb.1812.

Grefen, C., Donald, N., Hashimoto, K., Kudla, J., Schumacher, K., and Blatt, M.R. (2010). A ubiquitin-10 promoter-based vector set for fluorescent protein tagging facilitates temporal stability and

native protein distribution in transient and stable expression studies. Plant J **64**:355-365. 10.1111/j.1365-313X.2010.04322.x.

Grove, T.Z., Cortajarena, A.L., and Regan, L. (2008). Ligand binding by repeat proteins: natural and designed. Curr Opin Struct Biol **18**:507-515. 10.1016/j.sbi.2008.05.008.

Gualberto, J.M., and Newton, K.J. (2017). Plant mitochondrial genomes: Dynamics and mechanisms of mutation. Annu Rev Plant Biol **68**:225-252. 10.1146/annurev-arplant-043015-112232.

Guerrero-Castillo, S., Baertling, F., Kownatzki, D., Wessels, H.J., Arnold, S., Brandt, U., and Nijtmans, L. (2017). The assembly pathway of mitochondrial respiratory chain complex I. Cell Metab **25**:128-139. 10.1016/j.cmet.2016.09.002.

Guillaumot, D., Lopez-Obando, M., Baudry, K., Avon, A., Rigaill, G., Falcon de Longevialle, A., Broche, B., Takenaka, M., Berthomé, R., De Jaeger, G., et al. (2017). Two interacting PPR proteins are major Arabidopsis editing factors in plastid and mitochondria. Proc Natl Acad Sci U S A **114**:8877-8882. 10.1073/pnas.1705780114.

Gully, B.S., Cowieson, N., Stanley, W.A., Shearston, K., Small, I.D., Barkan, A., and Bond, C.S. (2015). The solution structure of the pentatricopeptide repeat protein PPR10 upon binding atpH RNA. Nucleic Acids Res **43**:1918-1926. 10.1093/nar/gkv027.

Guo, W., and Mower, J.P. (2013). Evolution of plant mitochondrial intron-encoded maturases: frequent lineage-specific loss and recurrent intracellular transfer to the nucleus. J Mol Evol **77**:43-54. 10.1007/s00239-013-9579-7.

Harrison, T., Ruiz, J., Sloan, D.B., Ben-Hur, A., and Boucher, C. (2016). aPPRove: An HMM-Based Method for accurate prediction of RNA-pentatricopeptide repeat protein binding events. PloS ONE **11**:e0160645-e0160645. 10.1371/journal.pone.0160645.

He, S., Sun, Y., Yang, Q., Zhang, X., Huang, Q., Zhao, P., Sun, M., Liu, J., Qian, W., Qin, G., et al. (2017). A novel imprinted gene NUWA controls mitochondrial function in early seed development in Arabidopsis. PLoS Genet **13**:e1006553. 10.1371/journal.pgen.1006553.

Hofacker, I.L., Fekete, M., and Stadler, P.F. (2002). Secondary structure prediction for aligned RNA sequences. J Mol Biol **319**:1059-1066.

Hooper, C.M., Castleden, I.R., Tanz, S.K., Aryamanesh, N., and Millar, A.H. (2017). SUBA4: the interactive data analysis centre for Arabidopsis subcellular protein locations. Nucleic Acids Res **45**:D1064-D1074. 10.1093/nar/gkw1041.

Hruz, T., Laule, O., Szabo, G., Wessendorp, F., Bleuler, S., Oertle, L., Widmayer, P., Gruissem, W., and Zimmermann, P. (2008). Genevestigator V3: a reference expression database for the meta-analysis of transcriptomes. Adv Bioinformatics **2008**:420747-420751.

Jumper, J., Evans, R., Pritzel, A., Green, T., Figurnov, M., Ronneberger, O., Tunyasuvunakool, K., Bates, R., Žídek, A., Potapenko, A., et al. (2021). Highly accurate protein structure prediction with AlphaFold. Nature **596**:583-589. 10.1038/s41586-021-03819-2.

Katoh, K., Rozewicki, J., and Yamada, K.D. (2017). MAFFT online service: multiple sequence alignment, interactive sequence choice and visualization. Brief Bioinform **20**:1160–1166. 10.1093/bib/bbx108.

Katz, A., Oliva, M., Mosquna, A., Hakim, O., and Ohad, N. (2004). FIE and CURLY LEAF polycomb proteins interact in the regulation of homeobox gene expression during sporophyte development. Plant J **37**:707-719. 10.1111/j.1365-313x.2003.01996.x.

Kenrick, P., Wellman, C.H., Schneider, H., and Edgecombe, G.D. (2012). A timeline for terrestrialization: consequences for the carbon cycle in the Palaeozoic. Philos Trans R Soc Lond B Biol Sci **367**:519-536. 10.1098/rstb.2011.0271.

Keren, I., Klipcan, L., Bezawork-Geleta, A., Kolton, M., Shaya, F., and Ostersetzer-Biran, O. (2008). Characterization of the molecular basis of group II intron RNA recognition by CRS1-CRM domains. J Biol Chem **283**:23333-23342. 10.1074/jbc.M710488200.

Keren, I., Tal, L., Colas des Francs-Small, C., Araújo, W.L., Shevtsov, S., Shaya, F., Fernie, A.R., Small, I., and Ostersetzer-Biran, O. (2012). nMAT1, a nuclear-encoded maturase involved in the *trans*-

splicing of *nad1* intron 1, is essential for mitochondrial complex I assembly and function. Plant J **71**:413-426. 10.1111/j.1365-313X.2012.04998.x.

Keren, I., Bezawork-Geleta, A., Kolton, M., Maayan, I., Belausov, E., Levy, M., Mett, A., Gidoni, D., Shaya, F., and Ostersetzer-Biran, O. (2009). AtnMat2, a nuclear-encoded maturase required for splicing of group-II introns in Arabidopsis mitochondria. RNA **15**:2299-2311. 10.1261/rna.1776409.

Kuhn, K., Obata, T., Feher, K., Bock, R., Fernie, A.R., and Meyer, E.H. (2015). Complete mitochondrial complex I deficiency induces an up-regulation of respiratory fluxes that is abolished by traces of functional complex I. Plant Physiol **168**:1537-1549. 10.1104/pp.15.00589.

Lambowitz, A.M., and Belfort, M. (2015). Mobile bacterial group II introns at the crux of eukaryotic evolution. Microbiol Spectr **3**:1-26.

Law, S.R., Narsai, R., Taylor, N.L., Delannoy, E., Carrie, C., Giraud, E., Millar, A.H., Small, I., and Whelan, J. (2012). Nucleotide and RNA metabolism prime translational initiation in the earliest events of mitochondrial biogenesis during Arabidopsis germination. Plant Physiol **158**:1610-1627. 10.1104/pp.111.192351.

Lee, K., Park, S.J., Colas des Francs-Small, C., Whitby, M., Small, I., and Kang, H. (2019). The coordinated action of PPR4 and EMB2654 on each intron half mediates trans-splicing of rps12 transcripts in plant chloroplasts. The Plant Journal **100**:1193-1207. https://doi.org/10.1111/tpj.14509.

Li-Pook-Than, J., and Bonen, L. (2006). Multiple physical forms of excised group II intron RNAs in wheat mitochondria. Nucleic Acids Res **34**:2782-2790. 10.1093/nar/gkl328.

Li-Pook-Than, J., Carrillo, C., and Bonen, L. (2004). Variation in mitochondrial transcript profiles of protein-coding genes during early germination and seedling development in wheat. Curr Genet **46**:374–380.

Li, S., Liu, J., Liu, Z., Li, X., Wu, F., and He, Y. (2014). HEAT-INDUCED TAS1 TARGET1 mediates thermotolerance via HEAT STRESS TRANSCRIPTION FACTOR A1a–directed pathways in Arabidopsis. Plant Cell **26**:1764-1780. 10.1105/tpc.114.124883.

Ligas, J., Pineau, E., Bock, R., Huynen, M.A., and Meyer, E.H. (2019). The assembly pathway of complex I in *Arabidopsis thaliana*. Plant J **97**:447-459. 10.1111/tpj.14133.

Liu, H., Wang, X., Wang, G., Cui, P., Wu, S., Ai, C., Hu, N., Li, A., He, B., Shao, X., et al. (2021). The nearly complete genome of *Ginkgo biloba* illuminates gymnosperm evolution. Nat Plants **7**:748-756. 10.1038/s41477-021-00933-x.

Lurin, C., Andres, C., Aubourg, S., Bellaoui, M., Bitton, F., Bruyere, C., Caboche, M., Debast, C., Gualberto, J., Hoffmann, B., et al. (2004). Genome-wide analysis of Arabidopsis pentatricopeptide repeat proteins reveals their essential role in organelle biogenesis. Plant Cell **16**:2089-2103.

Manavski, N., Guyon, V., Meurer, J., Wienand, U., and Brettschneider, R. (2012). An essential pentatricopeptide repeat protein facilitates 5' maturation and translation initiation of *rps3* mRNA in maize mitochondria. Plant Cell **24**:3087-3105. 10.1105/tpc.112.099051.

Martin, W., and Koonin, E.V. (2006). Introns and the origin of nucleus-cytosol compartmentalization. Nature **440**:41-45. Doi 10.1038/Nature04531.

Meinke, D.W. (2020). Genome-wide identification of EMBRYO-DEFECTIVE (EMB) genes required for growth and development in Arabidopsis. New Phytol **226**:306-325. https://doi.org/10.1111/nph.16071.

Meyer, E.H., Tomaz, T., Carroll, A.J., Estavillo, G., Delannoy, E., Tanz, S.K., Small, I.D., Pogson, B.J., and Millar, A.H. (2009). Remodeled respiration in *ndufs4* with low phosphorylation efficiency suppresses Arabidopsis germination and growth and alters control of metabolism at night. Plant Physiol **151**:603-619. 10.1104/pp.109.141770.

Millar, A.H., Whelan, J., Soole, K.L., and Day, D.A. (2011). Organization and regulation of mitochondrial respiration in plants. Annu Rev Plant Biol **62**:79-104. doi:10.1146/annurev-arplant-042110-103857.

Mizrahi, R., Shevtsov-Tal, S., and Ostersetzer-Biran, O. (2022). Group II intron-encoded proteins (IEPs/maturases) as key regulators of Nad1 expression and Complex I biogenesis in land plant mitochondria. Genes **13:**1-16. 10.3390/genes13071137.

Møller, I.M., Rasmusson, A.G., and Van Aken, O. (2021). Plant mitochondria – past, present and future. Plant J **108**:912-959. https://doi.org/10.1111/tpj.15495.

Nakagawa, N., and Sakurai, N. (2006). A mutation in At-nMat1a, which encodes a nuclear gene having high similarity to group II Intron maturase, causes impaired splicing of mitochondrial *nad4* transcript and altered carbon metabolism in *Arabidopsis thaliana*. Plant Cell Physiol **47**:772-783. 10.1093/pcp/pcj051.

Narsai, R., Law, S.R., Carrie, C., Xu, L., and Whelan, J. (2011). In depth temporal transcriptome profiling reveals a crucial developmental switch with roles for RNA processing and organelle metabolism that are essential for germination in *Arabidopsis thaliana*. Plant Physiol **157**:1342-1362. 10.1104/pp.111.183129.

O'Malley, R.C., Barragan, C.C., and Ecker, J.R. (2015). A user's guide to the Arabidopsis T-DNA insertion mutant collections. Methods Mol Biol **1284**:323-342. 10.1007/978-1-4939-2444-8_16.

Ostersetzer-Biran, O. (2016). Respiratory complex I and embryo development. J Exp Bot **67**:1205-1207. 10.1093/jxb/erw051.

Ostersetzer, O., Cooke, A.M., Watkins, K.P., and Barkan, A. (2005). CRS1, a chloroplast group II Intron splicing factor, promotes intron folding through specific interactions with two intron domains. Plant Cell **17**:241-255. 10.1105/tpc.104.027516.

Petersen, G., Cuenca, A., Moller, I.M., and Seberg, O. (2015). Massive gene loss in mistletoe (*Viscum, Viscaceae*) mitochondria. Sci Rep **5**:1-7. 10.1038/srep17588.

Petersen, S. (2007). Automated protein purification using His-tagged affinity chromatography with the Profinia protein purification system. FASEB J **21**:LB19-LB19. https://doi.org/10.1096/fasebj.21.6.LB19-c.

Pfalz, J., Bayraktar, O.A., Prikryl, J., and Barkan, A. (2009). Site-specific binding of a PPR protein defines and stabilizes 5' and 3' mRNA termini in chloroplasts. EMBO J **28**:2042.

Piccirilli, J.A., and Staley, J.P. (2016). Reverse transcriptases lend a hand in splicing catalysis. Nat Struct Mol Biol **23**:507-509. 10.1038/nsmb.3242.

Pineau, B., Layoune, O., Danon, A., and De Paepe, R. (2008). L-galactono-1,4-lactone dehydrogenase is required for the accumulation of plant respiratory complex I. J Biol Chem **283**:32500-32505. 10.1074/jbc.M805320200.

Popov, V.N., Syromyatnikov, M.Y., Fernie, A.R., Chakraborty, S., Gupta, K.J., and Igamberdiev, A.U. (2020). The uncoupling of respiration in plant mitochondria: keeping reactive oxygen and nitrogen species under control. J Exp Bot **72**:793-807. 10.1093/jxb/eraa510.

Prikryl, J., Rojas, M., Schuster, G., and Barkan, A. (2011). Mechanism of RNA stabilization and translational activation by a pentatricopeptide repeat protein. Proc Natl Acad Sci U S A **108**:415-420. DOI 10.1073/pnas.1012076108.

Pucker, B., Kleinbölting, N., and Weisshaar, B. (2021). Large scale genomic rearrangements in selected *Arabidopsis thaliana* T-DNA lines are caused by T-DNA insertion mutagenesis. bioRxiv:2021.2003.2003.433755. 10.1101/2021.03.03.433755.

Qi, W., Yang, Y., Feng, X., Zhang, M., and Song, R. (2017). Mitochondrial function and maize kernel development requires Dek2, a pentatricopeptide repeat protein involved in *nad1* mRNA splicing. Genetics **205**:239-249. 10.1534/genetics.116.196105.

Qu, G., Kaushal, P.S., Wang, J., Shigematsu, H., Piazza, C.L., Agrawal, R.K., Belfort, M., and Wang, H.W. (2016). Structure of a group II intron in complex with its reverse transcriptase. Nat Struct Mol Biol **23**:549-557. 10.1038/nsmb.3220.

Royan, S., Gutmann, B., Colas des Francs-Small, C., Honkanen, S., Schmidberger, J., Soet, A., Sun, Y.K., Vincis Pereira Sanglard, L., Bond, C.S., and Small, I. (2021). A synthetic RNA editing factor edits its target site in chloroplasts and bacteria. Commun Biol **4**:1-10. 10.1038/s42003-021-02062-9.

Ruwe, H., and Schmitz-Linneweber, C. (2012). Short non-coding RNA fragments accumulating in chloroplasts: footprints of RNA binding proteins? Nucleic Acids Res **40**:3106-3116. 10.1093/nar/gkr1138.

Ruwe, H., Wang, G., Gusewski, S., and Schmitz-Linneweber, C. (2016). Systematic analysis of plant mitochondrial and chloroplast small RNAs suggests organelle-specific mRNA stabilization mechanisms. Nucleic Acids Res **44**:7406-7417. 10.1093/nar/gkw466.

Salinas-Giegé, T., Giegé, R., and Giegé, P. (2015). tRNA biology in mitochondria. Int J Mol Sci **16**:4518-4559. 10.3390/ijms16034518.

Schertl, P., and Braun, H.P. (2014). Respiratory electron transfer pathways in plant mitochondria. Frontiers in plant science **5**:163. 10.3389/fpls.2014.00163.

Schmitz-Linneweber, C., Lampe, M.-K., Sultan, L.D., and Ostersetzer-Biran, O. (2015). Organellar maturases: A window into the evolution of the spliceosome. BBA - Bioenergetics **1847**:798-808. http://dx.doi.org/10.1016/j.bbabio.2015.01.009.

Schwarzländer, M., König, A.-C., Sweetlove, L.J., and Finkemeier, I. (2012). The impact of impaired mitochondrial function on retrograde signalling: a meta-analysis of transcriptomic responses. J Exp Bot **63**:1735-1750. 10.1093/jxb/err374.

Senkler, J., Senkler, M., Eubel, H., Hildebrandt, T., Lengwenus, C., Schertl, P., Schwarzländer, M., Wagner, S., Wittig, I., and Braun, H.-P. (2017). The mitochondrial complexome of *Arabidopsis thaliana*. Plant J **89**:1079-1092. doi:10.1111/tpj.13448.

Shen, C., Wang, X., Liu, Y., Li, Q., Yang, Z., Yan, N., Zou, T., and Yin, P. (2015). Specific RNA recognition by designer pentatricopeptide repeat protein. Mol Plant **8**:667-670. 10.1016/j.molp.2015.01.001.

Shen, C., Zhang, D., Yan, J., Zhang, Q., Hong, S., Yang, Y., Yao, Y., Yin, P., and Zou, T. (2019). Delineation of pentatricopeptide repeat codes for target RNA prediction. Nucleic Acids Res **47**:3728-3738. 10.1093/nar/gkz075.

Shevtsov-Tal, S., Best, C., Matan, R., Chandran, S.A., Brown, G.G., and Ostersetzer-Biran, O. (2021). nMAT3 is an essential maturase splicing factor required for holo-complex I biogenesis and embryo development in *Arabidopsis thaliana* plants. Plant J **106**:1128-1147. 10.1111/tpj.15225.

Skippington, E., Barkman, T.J., Rice, D.W., and Palmer, J.D. (2015). Miniaturized mitogenome of the parasitic plant Viscum scurruloideum is extremely divergent and dynamic and has lost all nad genes. Proc Natl Acad Sci U S A **112**:E3515-E3524. 10.1073/pnas.1504491112.

Sloan, D., Alverson, A., Chuckalovcak, J., Wu, M., McCauley, D., Palmer, J., and Taylor, D. (2012). Rapid evolution of enormous, multichromosomal genomes in flowering plant mitochondria with exceptionally high mutation rates. PLoS Biol **10**:e1001241.

Sloan, D.B., Wu, Z., and Sharbrough, J. (2018). Correction of persistent errors in Arabidopsis reference mitochondrial genomes. Plant Cell **30**:525-527. 10.1105/tpc.18.00024.

Small, I.D., and Peeters, N. (2000). The PPR motif - a TPR-related motif prevalent in plant organellar proteins. Trends Biochem Sci **25**:45-47.

Soto, D., Cordoba, J.P., Villarreal, F., Bartoli, C., Schmitz, J., Maurino, V.G., Braun, H.P., Pagnussat, G.C., and Zabaleta, E. (2015). Functional characterization of mutants affected in the carbonic anhydrase domain of the respiratory complex I in *Arabidopsis thaliana*. Plant J **83**:831-844. 10.1111/tpj.12930.

Sultan, L.D., Mileshina, D., Grewe, F., Rolle, K., Abudraham, S., Głodowicz, P., Khan Niazi, A., keren, I., Shevtsov, S., Klipcan, L., et al. (2016). The reverse-transcriptase/RNA-maturase protein MatR is required for the splicing of various group II introns in Brassicaceae mitochondria. Plant Cell **28**:2805-2829. 10.1105/tpc.16.00398.

Takenaka, M., Zehrmann, A., Brennicke, A., and Graichen, K. (2013). Improved Computational Target Site Prediction for Pentatricopeptide Repeat RNA Editing Factors. PLoS ONE **8**:e65343. 10.1371/journal.pone.0065343.

Thorvaldsdottir, H., Robinson, J.T., and Mesirov, J.P. (2013). Integrative Genomics Viewer (IGV): high-performance genomics data visualization and exploration. Brief Bioinform **14**:178-192. 10.1093/bib/bbs017.

Unseld, M., Marienfeld, J.R., Brandt, P., and Brennicke, A. (1997). The mitochondrial genome of *Arabidopsis thaliana* contains 57 genes in 366,924 nucleotides. Nature Genet **15**:57-61.

Wang, C., Blondel, L., Quadrado, M., Dargel-Graffin, C., and Mireau, H. (2022). Pentatricopeptide repeat protein MITOCHONDRIAL STABILITY FACTOR 3 ensures mitochondrial RNA stability and embryogenesis. Plant Physiol **190**:669-681. 10.1093/plphys/kiac309.

Wang, G., Zhong, M., Shuai, B., Song, J., Zhang, J., Han, L., Ling, H., Tang, Y., Wang, G., and Song, R. (2017). E+ subgroup PPR protein defective kernel 36 is required for multiple mitochondrial transcripts editing and seed development in maize and Arabidopsis. New Phytol **214**:1563-1578. https://doi.org/10.1111/nph.14507.

Weigel, D., and Glazebrook, J. (2006). Root transformation of Arabidopsis. CSH protocols **2006**10.1101/pdb.prot4671.

Woodson, J.D., and Chory, J. (2008). Coordination of gene expression between organellar and nuclear genomes. Nat Rev Genet **9**:383-395. http://www.nature.com/nrg/journal/v9/n5/suppinfo/nrg2348_S1.html.

Yagi, Y., Hayashi, S., Kobayashi, K., Hirayama, T., and Nakamura, T. (2013). Elucidation of the RNA recognition code for pentatricopeptide repeat proteins involved in organelle RNA editing in plants. PLoS ONE **8**:e57286.

Yan, J., Yao, Y., Hong, S., Yang, Y., Shen, C., Zhang, Q., Zhang, D., Zou, T., and Yin, P. (2019). Delineation of pentatricopeptide repeat codes for target RNA prediction. Nucleic Acids Res **47**:3728-3738. 10.1093/nar/gkz075.

Yang, L., Garcia Canaveras, J.C., Chen, Z., Wang, L., Liang, L., Jang, C., Mayr, J.A., Zhang, Z., Ghergurovich, J.M., Zhan, L., et al. (2020). Serine catabolism feeds NADH when respiration is impaired. Cell Metab **31**:809-821.e806. https://doi.org/10.1016/j.cmet.2020.02.017.

Yin, P., Li, Q., Yan, C., Liu, Y., Liu, J., Yu, F., Wang, Z., Long, J., He, J., Wang, H.-W., et al. (2013). Structural basis for the modular recognition of single-stranded RNA by PPR proteins. Nature **504**:168. 10.1038/nature12651.

Yu, D., Jiang, L., Gong, H., and Liu, C.-M. (2012). EMBRYONIC FACTOR 19 encodes a pentatricopeptide repeat protein that is essential for the initiation of zygotic embryogenesis in Arabidopsis. J Integr Plant Biol **54**:55-64. https://doi.org/10.1111/j.1744-7909.2011.01089.x.

Zhao, C., and Pyle, A.M. (2016). Crystal structures of a group II intron maturase reveal a missing link in spliceosome evolution. Nat Struct Mol Biol **23**:558-565. 10.1038/nsmb.3224.

Zhao, C., and Pyle, A.M. (2017). Structural Insights into the Mechanism of Group II Intron Splicing. Trends Biochem Sci **42**:470-482. 10.1016/j.tibs.2017.03.007.

Zimmerly, S., and Semper, C. (2015). Evolution of group II introns. Mobile DNA **6**:1-19. 10.1186/s13100-015-0037-5.

Zimmermann, P., Hirsch-Hoffmann, M., Hennig, L., and Gruissem, W. (2004). GENEVESTIGATOR. Arabidopsis microarray database and analysis toolbox. Plant Physiol **136**:2621-2632.

Zmudjak, M., and Ostersetzer-Biran, O. (2017). RNA metabolism and transcript regulation (Chichester John Wiley & Sons, Ltd). doi:10.1002/9781118906583.ch6, https://onlinelibrary.wiley.com/doi/abs/10.1002/9781118906583.ch6.

Zmudjak, M., Colas des Francs-Small, C., Keren, I., Shaya, F., Belausov, E., Small, I., and Ostersetzer-Biran, O. (2013). mCSF1, a nucleus-encoded CRM protein required for the processing of many mitochondrial introns, is involved in the biogenesis of respiratory complexes I and IV in Arabidopsis. New Phytol **199**:379-394. 10.1111/nph.12282.

Zuker, M. (2003). Mfold web server for nucleic acid folding and hybridization prediction. Nucl Acids Res **31**:3406-3415. 10.1093/nar/gkg595.

Table 1. List of *Arabidopsis* PPR-related *emb* mutants with predicted or established roles in mitogenome expression or mtRNA metabolism.

Gene I.D.	Gene symbol	PPR group	Cellular location[*1]	Gene function	References
At4g20090	***MSP1/ EMB1025***	**P**	**mit**	**Altered *nad1.1* processing**	**This study, (Cushing et al., 2005)**
At1g05600	*EMB3101*	P	(mit)	n.d.[*2]	
At1g10270	*GRP23*	P	nucl/mit	nuclear transcription (interacts with RNA pol II), mito's functions?	(Ding et al., 2006; Narsai et al., 2011; Senkler *et al.*, 2017)
At1g74900	*OTP43*	P	mit	splicing of *nad1* i1	(Falcon de Longevialle *et al.*, 2007)
At1g77360	*APPR6*	P	mit	5'-end processing, translational initiation of *rps3* RNA	(Manavski *et al.*, 2012)
At1g79490	*EMB2217*	P	(mit)	n.d.	(Narsai *et al.*, 2011)
At2g01390	*EMB3111*	P	(mit)	n.d.	(Narsai *et al.*, 2011)
At2g02150	*EMB2794*	P	(mit/clp)	n.d.	
At2g15690	*DYW2*	DYW	(mit)	Provides the missing cytidine deaminase activity to the E+ PPR proteins	(Guillaumot et al., 2017)
At2g32230	*PRORP1*	P	mit/clp	RNase P-like (5' cleavage of pre-tRNAs)	(Gobert et al., 2010)
At2g35030	*COD1*	E+	mit	mitochondrial RNA editing	(Dahan *et al.*, 2014)
At3g22670	*EMP10*	P	(mit)	homolog of ZmEMP10 (putative splicing factor)	(Cai et al., 2017)
At3g49240	*NUWA*	P	mit	May bridge and stabilize the interaction between PPR-E+ and DYW2 proteins, or regulates mtRNA translation	(He et al., 2017)
At4g21190	*EMB1417*	P	(mit)	n.d.	
At4g21300	*DEK36*	E+	mit	mitochondrial RNA editing	(Wang *et al.*, 2017)
At4g33990	*EMB2758*	DYW	(mit)	n.d.	
At5g39680	*EMB2744*	DYW	(mit)	n.d.	
At5g39710	*EMB2745*	P	(mit)	n.d. (regulated by miR400?)	(Li et al., 2014)
At1g13800	*FAC19*	P	(mit)	possibly RNA editing	(Yu et al., 2012)

*[1] - quotes indicate to predicted intracellular locations by the ExPASy portal (https://www.expasy.org) and the SUBAcon server (Hooper et al., 2017) (mitochondrial, mit; chloroplast, clp; nucleus, nucl; cytosolic, cyto).
*[2] - n.d., not determined.

Figure legends

Figure 1. *AT4G20090* gene product encodes an essential mitochondria-localized PPR protein. (A) Scheme of *MSP1* (*AT4G20090*) gene structure. In silico analysis suggest the presence of at least 11 repeats (P4 to P14) of the conserved P-class PPR motif, and putative additional 3 PPRs (P1 to P3) at the N-terminus and the PPR domain P15 at the C-terminus. The positions of the predicted mitochondrial targeting signal (mTS) and the T-DNA insertion in SALK line 142675 (*msp1-1*) within the coding sequence of *MSP1* are outlined above the sequence. (B) GFP localization analyses. *Arabidopsis* root tissue culture cells were agroinfiltrated with pCAMBIA 2300 vectors containing GFP sequence fused in-frame to the plastidial Rubisco small subunit (*RBCS*, *AT1G67090*) and *MSP1* (*AT4G20090*) coding sequences, under the control of the *UBIQUTIN-10* (*AT4G05320*) promoter (Grefen et al., 2010). The figure shows bright-field images (grayscale) and confocal GFP signals (green), MitoTracker marker (red) and overlain GFP + MitoTracker images obtained with each construct. (C) Mature siliques obtained from heterozygous *msp1-1* (SALK-142675) lines. Arrows indicate homozygous mutant seeds. Numbers indicate seeds which contain embryos arrested at the late heart or torpedo stages ("1"), or aborted seeds with dead embryos ("2"). (D) White seeds (containing homozygous *msp1* embryos) and green seeds (containing heterozygous or wild-type embryos) obtained from the immature siliques of heterozygous *msp1-1* plants. Images taken with differential interference contrast (Nomarski) microscopy. (E) Seeds collected under sterile conditions from surface sterilized immature siliques of Col-0 and heterozygous *msp1-1* plants, were sown on petri dishes containing MS-Agar supplemented with 1% sucrose and vitamins (see Materials and methods) and grown in an *Arabidopsis* growth chamber under standard conditions. 6-week-old *msp1-1* (F) or Col-0 (G) plantlets grown the MS-plates (L6 growth stage), were transferred to liquid MS-media supplemented with 1% sucrose and vitamins (see Materials and Methods). These often develop short leaves with limited stems resulting with a bushy-like phenotype (H) that was previously noted by Dahan *et al.* (2014). (I) Five-month-old rosettes of homozygous *MSP1-1* plants grown on soil at 22°C under short-day conditions.

Figure 2. Transcript abundance in *msp1* mutants.

RT-qPCR analyses of mitochondrial protein-coding genes was performed essentially as described previously (Cohen et al., 2014; Shevtsov-Tal *et al.*, 2021; Sultan *et al.*, 2016; Zmudjak et al., 2013).

RNA extracted from 3-week-old seedlings of wild-type plants, 5-month-old rescued *msp1-1* mutant plantlets and plantlets obtained from the immature seeds of Col-0 plants containing embryos at the heart stage (Fig. 1D) was reverse-transcribed and the relative steady-state levels of cDNAs corresponding to the different organellar transcripts were evaluated by qPCR with primers which specifically amplified mRNAs (Table S2). Histograms showing the relative mRNAs levels (log2 ratios) in (1) rescued homozygous *msp1-1* and germinated embryos of wild-type (Col-0-heart) plantlets, or (2) heterozygous *msp1-1* (*htz*) plants and *msp1:35S-MSP1* (line #18, Fig. S3) complemented plants, versus those of 3-week-old MS-grown wild-type (Col-0) plants. Transcripts analyzed in these assays include the NADH dehydrogenase (CI) subunits *nad1* exons a-b, b-c, c-d, d-e, *nad2* exons a-b, b-c, c-d, d-e, *nad3*, *nad4* exons a-b, b-c, c-d, *nad4L*, *nad5* exons a-b, b-c, c-d, d-e, the intronless *nad6* subunit, *nad7* exons a-b, b-c, c-d, d-e, and *nad9*, the complex III *cob* subunit, cytochrome oxidase (complex IV) *cox1*, *cox2* exons a-b and *cox3* subunits, the ATP synthase (i.e., complex V) subunits *atp1*, *atp4*, *atp6*, *atp8* and *atp9*, genes encoding the cytochrome c maturation (*ccm*) factors, *ccmB*, *ccmC*, *ccmFn1*, *ccmFn2* and *ccmFc* exons a-b, the ribosomal subunits *rpl2* exons a-b, *rps3* exons a-b, *rps4*, *rps7*, *rps12*, *rpl16*, *rrn26*, and the *mttB* gene. Arrows indicate genes that are interrupted by group II intron sequences in *Arabidopsis* mitochondria (Sloan *et al.*, 2018), while asterisks indicate transcripts where the mRNA levels were reduced in *msp1-1* plants, but not of the rescued Col-0 seedlings. The values are means of 15 reactions corresponding to five biological replicates (error bars indicate one standard deviation).

Figure 3. Transcription profiles of *msp1-1* mutant-line by RNA-seq analyses.

Total RNA extracted from Col-0 and *msp1-1* plantlets was used to generate Illumina-sequencing (NovaSeq 6000, 150 bp paired-end) libraries (BioProjects PRJNA704631 and PRJNA768306). (A) Heatmap illustrating the relative expression levels between two wild-type (Col-0) plants and five mutant (*msp1*) lines of each individual exon. Darker colors indicate to reduced exon levels in *msp1 vs* the Col-0 plants. (B) Ratio of read coverage between Col-0 and *msp1* across the whole genome. (C) RNA-seq data of *Arabidopsis* mitochondrial *nad1.1* transcript (BioProject PRJNA768306, corresponding to 3 individual Col-0 plants), showing the read depth along the *nad1.1* sequence (containing exon 'a' and domains 1-4 of *nad1* intron 1.1). The predicted MSP1 RNA-binding site is indicated below the plot.

Figure 4. MSP1 is associated with a specific intronic region in *nad1* i1 and eliminates 3′-end exoribonucleolytic degradation by PNPase, in-vitro.

(A) The association between rMSP1 and *nad1* pre-RNA transcripts was analyzed by incubating increasing amounts of the protein (0 – 80 μM) with in-vitro transcribed labeled RNAs. Binding was analyzed by filtration of the RNA-protein complex filter binding assays (Barkan et al., 2007; Keren *et al.*, 2008; Ostersetzer *et al.*, 2005). A raw slot-blot data is shown from representative experiments on top of the graph. The graph shows the binding activity of MSP1 to *nad1* i1in the presence or absence of competitor RNA-oligos, or to *nad1* i1 ΔMBS. GST was used as a control for the *nad1* i1 binding assays. The values are means of four independent measurements (error bars indicate one standard deviation). (B) MSP1-mediated protection of *nad1* i1 from 3′→5′ exonuclease activity. Polynucleotide phosphorylase (PNPase)-protection assays (Prikryl *et al.*, 2011) were performed with 5′-end ^{32}P-labeled RNAs. RNAs corresponding to nad1 i1 and *nad1* i1 ΔMBS were denatured (i.e., 2 min at 95 °C, and snap cooled on ice), and then incubated with rMSP1 prior to their use in the PNPase reaction assays. The *nad1* i1 stabilization effects of rMSP1 were further analyzed in the presence of the exonucleases benzonase (cleaves all forms of DNA or RNA into 3 to 5 bases in length) or RNase-A (cleaves the phosphodiester bond between the 5'-ribose of a nucleotide and the phosphate group attached to the 3'-ribose of an adjacent pyrimidine nucleotide). The reactions were stopped by heating the samples in RNA sample buffer containing 60% formamide, and the RNAs were then resolved on 10% AA gels containing 7M urea in 1×TBE buffer. The position of protected *nad1* i1 terminus was determined from the size of the corresponding end-labeled RNA.

Figure 5. Analyses of the organellar protein profiles of wild-type and *msp1-1* plants.

(A) Immunoblots with proteins (about 50 μg) of mitochondrial enriched membranous fractions (Pineau *et al.*, 2008; Sultan *et al.*, 2016), isolated from MS-grown Col-0 and rescued *msp1-1* plants. The blots were probed with polyclonal antibodies (Table S4) raised against the NADH-oxidoreductase subunit 1 (Nad1), γ-carbonic anhydrase-like subunit 2 (CA2) and Nad9 proteins. Detection was carried out by chemiluminescence assays after incubation with HRP-conjugated secondary antibody (note that the dashed box in the Nad1 blot corresponds to a 1.5x magnified image copied below the blot).

(B) Blue native (BN) PAGE analyses of crude organellar membranous fractions. An aliquot equivalent to 40 mg of crude *Arabidopsis* mitochondria extracts, obtained from wild-type plants, *msp1* mutant-lines and complemented *msp1:35S-MSP1*, was solubilized with 5% (w/v) digitonin, and the organellar complexes were resolved by BN-PAGE. For immunodetection, the proteins were transferred from the native gels onto a PVDF membrane. The membranes probed with antibodies raised to complex I (CI) NADH-oxidoreductase subunit 9 (Nad9) and γ-carbonic anhydrase-like subunit 2 (CA2) proteins. In-gel CI activity assays were performed essentially as described previously (Eubel *et al.*, 2005). Arrows indicate to the native supercomplex I+III2 (~1,500 kDa) or holo-CI (~1,000 kDa), while I* indicates the presence of CI assembly intermediates.

Figure 6. phylogenetic distribution of MSP1 gene and its genetically-defined *nad1* intron 1 RNA target.

Genomic and organellar sequences available at the NCBI were used to search for *MSP1*-related PPR genes and *nad1* sequences in different plant clades, using The Basic Local Alignment Search Tool (BLAST). The results of the BLAST searches were integrated into the phylogenetic relationships among photosynthetic organisms, as indicated for the terrestrial flora (Delwiche and Cooper, 2015; Kenrick *et al.*, 2012). Branch lengths as illustrated do not represent phylogenetic distances and are intended to indicate instead relationships among different clades. Mitochondrial *nad1* intron 1 (*nad1* i1) and the nuclear *MSP1* genes are shown as circles and boxes, respectively. Black boxes (MSP1) and black circles (*nad1* i1 in a *trans*- or *cis*-configurations) show that corresponding sequences are present, whereas open boxes indicate that the gene is absent in the organisms belonging to a specific plant clade. Pattern fill indicates the presence of homologous sequences, whereas red crosses indicate the absence of the proposed MSP1 binding site.

Supplementary data

Figure S1. *MSP1* gene expression patterns at different tissues and during various developmental stages.

The expression patterns of *MSP1* were analyzed by publicly available microarray and high throughput sequencing databases, including (A) Genevestigator analysis toolbox (Hruz *et al.*,

2008; Zimmermann et al., 2004) and (B) The *Arabidopsis* Information Resource, TAIR; http://www.arabidopsis.org).

Figure S2. MSP1 protein structure and its predicated RNA biding site.

(A) The deduced amino acid sequence of MSP1. The predicted mitochondrial targeting sequence (36~37 amino acid long) is highlighted in magenta, with the cleavage sites indicated by box. Regions of low confidence are colored in grey. Predicted PPR motifs are indicated (domains of low scoring are highlighted in cyan and coded blue for regions of high confident). (B) Homology modeling of *Arabidopsis thaliana* (Col-0) MSP1. The 3D model of the MSP1 protein structure was obtained from AlphaFold server (Jumper *et al.*, 2021), using a per-residue confidence score (pLDDT) (indicated below the figure). The hypothetical 3D surface of MSP1 was visualized with PyMol. The "I" and "IV" panels represent ribbon structures at different angles, whereas "II" and "III" indicate the hypothetical surface of MSP1. The color code is red for negative values, white for near zero values and blue for positive values.

Figure S3. PCR screening of *msp1* plants.

(A) The nucleotide sequence of *MSP1* encoded by *AT4G20090*. Lower case indicates the 5' and 3' untranslated regions (UTRs), while uppercase letters represent the open reading frame of *MSP1* (as indicated by the TAIR database). The reported positions of T-DNA insertions in *msp1-1* (SALK-142675), SALK-018927 and SALK-070654 lines are indicated in the sequence of *MSP1*. PCR followed by sequencing suggest a double insertion event for the *msp1-1* line within the coding region of *MSP1* (see Table S6). Analyses of genomic PCR products spanning the reported T-DNA insertion junctions failed to support T-DNA insertions in the *MSP1* in SALK-lines 018927 and 070654. (B) PCR screening of germinated plantlets obtained from mature seeds of heterozygous *msp1-1* mutants, with primers designed to the *MSP1* gene and SALK T-DNA left border primer (LBb1.3) (Table S6). Arrows indicate the 465 bp and 541 bp products that correspond to the gene fragment and the *T-DNA-MSP1* insertional product, respectively. The nucleotide sequence of the precise insertion position of *msp1-1* is presented in Fig. S3. (C) PCR screening of homozygous *msp1-1* mutants carrying the 35S:*MSP1* transgene (*i.e.*, complemented lines). Specific primers used for the screening of complemented *msp1-1* lines are listed in Table S6.

Figure S4. The mitochondrial transcription profiles of *msp1-1*.

Figure S1. *MSP1* gene expression patterns at different tissues and during various developmental stages.

The expression patterns of *MSP1* were analyzed by publicly available microarray and high throughput sequencing databases, including (A) Genevestigator analysis toolbox (Hruz *et al.*, 2008; Zimmermann *et al.*, 2004) and (B) The *Arabidopsis* Information Resource, TAIR; http://www.arabidopsis.org).

Figure S2. MSP1 protein structure and its predicated RNA biding site.

(A) The deduced amino acid sequence of MSP1. The predicted mitochondrial targeting sequence (36~37 amino acid long) (Emanuelsson et al., 2000; Hooper *et al.*, 2017) is highlighted in magenta, with the cleavage sites indicated by box. Regions of low confidence are colored in grey. Predicted PPR motifs are indicated (domains of low scoring are highlighted in cyan and coded blue for regions of high confident). (B) Homology modeling of *Arabidopsis thaliana* (Col-0) MSP1. The 3D model of the MSP1 protein structure was obtained from AlphaFold server (Jumper *et al.*, 2021), using a per-residue confidence score (pLDDT) (indicated below the figure). The hypothetical 3D surface of MSP1 was visualized with PyMol. The "I" and "IV" panels represent ribbon structures at different angles, whereas "II" and "III" indicate the hypothetical surface of MSP1. The color code is red for negative values, white for near zero values and blue for positive values.

Figure S3. PCR screening of *msp1* plants.

(A) The nucleotide sequence of *MSP1* encoded by *AT4G20090*. Lower case indicates the 5' and 3' untranslated regions (UTRs), while uppercase letters represent the open reading frame of *MSP1* (as indicated by the TAIR database). The reported positions of T-DNA insertions in *msp1-1* (SALK-142675), SALK-018927 and SALK-070654 lines are indicated in the sequence of *MSP1*. PCR followed by sequencing suggest a double insertion event for the *msp1-1* line within the coding region of *MSP1* (see Table S6). Analyses of genomic PCR products spanning the reported T-DNA insertion junctions failed to support T-DNA insertions in the *MSP1* in SALK-lines 018927 and 070654. (B) PCR screening of germinated plantlets obtained from mature seeds of heterozygous *msp1-1* mutants, with primers designed to the *MSP1* gene and SALK T-DNA left border primer (LBb1.3) (Table S6). Arrows indicate the 465 bp and 541 bp products that correspond to the gene

fragment and the *T-DNA-MSP1* insertional product, respectively. The nucleotide sequence of the precise insertion position of *msp1-1* is presented in Fig. S3. (C) PCR screening of homozygous *msp1-1* mutants carrying the 35S:*MSP1* transgene (*i.e.*, complemented lines). Specific primers used for the screening of complemented *msp1-1* lines are listed in Table S6.

Figure S4. The mitochondrial transcription profiles of *msp1-1*.

(A) Transcriptomic data are shown for mtDNA loci corresponding to the *nad1.1* (nucleotides 81,785 - 83,966, indicated in blue color), *nad1.2* (nucleotides 58,315 - 60,868, indicated in green) and *nad1.3* (nucleotides 230,304 - 237,530, indicated in red) gene fragments. The *nad1.1* and *nad1.2* fragments are separated by domain 4 of intron 1, while the *nad1.2* and *nad1.3* transcription units are fragmented by domain 4 of intron 3. The structure of *nad1* i1 intron was modeled based on previous structural models of group II intron RNAs (Candales et al., 2011; Dai et al., 2003), structural analyses of bacterial MATs bound to their cognate group II intron RNAs (Piccirilli and Staley, 2016; Qu et al., 2016; Zhao and Pyle, 2016), and the secondary structure prediction algorithms MFOLD (Zuker, 2003) and Alifold (Hofacker et al., 2002). The figure includes 16 nucleotides of the 5' exon and 1,151 nucleotides of the 5'-part of the intron from transcript *nad1.1* (in blue color) plus 108 nucleotides of the 3' part of the intron and 11 nucleotides of the 3' exon from transcript *nad1.2* (in green color). Residue numbering begins at the first intron nucleotide (*i.e.*, 5'-part). Nucleotides predicted to be involved in the canonical group II intron tertiary interactions, including the IBS1-EBS1, IBS2-EBS2, α-α', β-β', γ-γ', δ-δ', ε-ε', ζ-ζ', κ-κ', λ-λ', θ-θ' and the η-η' interactions are indicated, while the predicted RNA binding site of MSP1 (5'- acaUACCAAAAGGUu, Fig. S5) is highlighted. The predicted bulged A cleavage site (Li-Pook-Than and Bonen, 2006) is indicated in bold red color in domain VI. (B) For the RNA-seq analyses, total mtRNA was extracted from individual Col-0 and embryo-rescued *msp1-1* plantlets (seven runs corresponding to 3 biological repeats), which was used to generate Illumina-sequencing libraries (BioProjects PRJNA704631 and PRJNA768306). The alignments between Col-0 or *msp1-1* plants(154) and the established *Arabidopsis* mtDNA (Sloan *et al.*, 2018) were visualized using the IGV genome browser (Thorvaldsdottir et al., 2013). Green and red (-strand) or blue and red (+strand) lines point to different mtRNA-editing (C-to-U conversions) events established for exon regions in *Arabidopsis* mitochondria (Sloan *et al.*, 2018). Arrows show the direction of transcription. Boxes represent different exons or ORF regions, while lines indicate to

group II intron regions. Dashed lines represent UTR regions (Best et al., 2020b). (C) Read coverage in the *nad1* exon-a region in Col-0 (blue) and *msp1* (orange) plants. Total RNA extracted from Col-0 and *msp1-1* plantlets was used to generate Illumina-sequencing (NovaSeq 6000, 150 bp paired-end) libraries (BioProjects PRJNA704631 and PRJNA768306).

Figure S5. Analysis of MSP1 RNA binding site.

(A) A combinatorial code for RNA recognition by the predicted MSP1 PPR motifs. Amino acids at positions 5 and the end of each domain act as specificity-determining residues (Barkan *et al.*, 2012; Cheng *et al.*, 2016; Takenaka et al., 2013). *In-silico* data (Cheng *et al.*, 2016; Harrison et al., 2016; Shen et al., 2019) indicate the preferred sequence 5'-UACCAAAAGGU for MSP1's PPR 4-11 motifs. (B) The PPRmatcher algorithm (Royan *et al.*, 2021), which aligns the predicated PPR motifs to every possible position in the mitogenome of Arabidopsis (i.e., ~720K positions) and scores each alignment based on the data in (Yan et al., 2019).

Figure S6. Expression and purification of a recombinant rMSP1 protein.

(A) The codon optimized region of the PPR domains 3 to 14 of MSP1 was cloned into pGEX-4T1, in-frame to GST in its N-terminus and a C-terminal 6xHis tag. The recombinant protein (rMSP1, 71,365 kDa) was expressed in *E. coli* (strain BL21 cells), and induced with 1.0 mM IPTG for 2 h at 37°C. The cells were pelleted, resuspended with in a 6M guanidine hydrochloride buffer, and lysed by a high-pressure chamber manifold. Non-soluble materials were removed by centrifugation. Immunoblots with anti-GST antibodies and protein MS-analysis confirmed the integrity of the over-expressed recombinant protein. (B) The rMSP1 was purified by Ni-NTA column under denaturing conditions, using the BioRad Profinia (Petersen, 2007) purification system and column kit.

Figure S7. The relative accumulation of organellar proteins and respiratory complexes in wild-type and *msp1-1* plants.

(A) Immunoblots with proteins (about 50 μg) of mitochondrial enriched membranous fractions (Pineau *et al.*, 2008; Sultan *et al.*, 2016), isolated from MS-grown Col-0 and rescued *msp1-1* plants. The blots were probed with polyclonal antibodies (Table S4) raised against Rieske iron-sulfur protein (RISP) of complex III (CIII), the cytochrome oxidase subunit 2 (Cox2) of complex

IV (CIV), mitochondrial Atp1 and ATP2 subunits of ATP-synthase (CV) and the mitochondrial voltage-dependent anion channel (VDAC, or porin). Detection was carried out by chemiluminescence assays after incubation with HRP-conjugated secondary antibody (note that the box in the RISP blot is a cropped image of the lanes that correspond to *msp1*, so that the heterozygous and homozygous lines are found at the same loading order as in the other blots; no other changes have been made to the original blots). (B) Analyses of the expression levels of various alternative oxidases (AOXs) and rotenone-insensitive NAD(P)H dehydrogenases (NDs) in *Arabidopsis* plants was performed by RT-qPCR, as described previously (Cohen *et al.*, 2014; Sultan *et al.*, 2016; Zmudjak *et al.*, 2013). RNA extracted from wild-type (Col-0) and embryo-rescued *msp1-1* mutant was reverse-transcribed, and the relative steady-state levels of cDNAs corresponding to the different *AOX* and *ND* transcripts were evaluated by qPCR with primers which specifically amplified their mRNAs (Table S2). The histogram shows the relative mRNAs levels in *msp1-1* and rescued Col-0 plantlets versus 3-week-old MS-grown Col-0 plants. (C) Blue native (BN) PAGE analyses of crude organellar membranous fractions. An aliquot equivalent to 40 mg of crude *Arabidopsis* mitochondria extracts, obtained from wild-type plants, *msp1* mutant-lines and complemented *msp1:35S-MSP1*, was solubilized with 5% (w/v) digitonin, and the organellar complexes were resolved by BN-PAGE. For immunodetection, the proteins were transferred from the native gels onto a PVDF membrane. The membranes probed with antibodies raised to Rieske iron-sulfur protein (RISP) of complex III (CIII), the cytochrome oxidase subunit 2 (Cox2) of complex IV (CIV), mitochondrial ATP2 subunit of ATP-synthase (CV) (Table S4), as indicated below each blot. Arrows indicate to the native supercomplex I+III2 (~1,500 kDa), III_2 (~500 kDa), CIV (~220 kDa) and CV (~600 kDa).

Figure S8. Relative accumulation and activity of respiratory CI in wild-type and *nmat1* plants.

BN-PAGE of crude organellar membranous fractions was performed generally as described previously (Pineau *et al.*, 2008). An aliquot equivalent to 40 mg of crude *Arabidopsis* mitochondria extracts, obtained from wild-type (Col-0) plants and *nmat1* mutants (Keren *et al.*, 2012; Nakagawa and Sakurai, 2006), was solubilized with 5% (w/v) digitonin and the organellar complexes were resolved by BN-PAGE. For immunodetection, the proteins were transferred from the native gels onto a PVDF membrane. The membranes were destained with ethanol before probing with specific

antibodies (Table S4), as indicated below each blot. *In-gel* complex I activity assays were performed essentially as described previously (Meyer*, et al.* 2009). Arrows indicate the native supercomplex I+III2 (~1,500 kDa) and holo-complex I (~1,000 kDa). The asterisks in the CA2 panel indicate the presence of partial CI assembly intermediates (I*), with calculated masses of about 800, 750, 700, 650, 600 and 350 kDa. Note that the four lanes in each of the immunoblots were loaded and separated on the same gels. We cropped the images to remove lanes corresponding to another mutant line. No other modifications were done to the original images.

Figure S9. Splicing efficiencies in *ca2* mutants.

The relative accumulation of mRNA and pre-RNA transcripts in wild-type and *ca2* plants (Ci Rdoba et al., 2019; Cordoba *et al.*, 2016; Fromm et al., 2016a; Fromm et al., 2016b; Soto et al., 2015), corresponding to the 23 group II intron sequences in *Arabidopsis*, was evaluated by RT-qPCR, essentially as described previously (Cohen *et al.*, 2014; Sultan *et al.*, 2016). RNA extracted from Col-0 and mutant plants was reverse-transcribed and the relative steady-state levels of cDNAs corresponding to the different organellar transcripts were evaluated by qPCR with primers which specifically amplified pre-RNAs and mRNAs. The histogram shows the splicing efficiencies as indicated by the log2 ratios of pre-RNA to mRNA transcript abundance in *ca2* mutants, compared with those of 3-week-old MS-grown wild-type plants. The values are means of six replicates (error bars indicate one standard deviation).

Figure S10. The predicted MSP1 binding site is highly conserved among different spermatophytes.

Alignment of homologous mitochondrial *nad1.1* sequences from *Arabidopsis thaliana (A.t.)*, *Ceratozamia hildae (C.h.)*, *Cycas taitungensis (C.t.)*, *Ginkgo biloba (G.b.)*, *Glycine max (G.ma.)*, *Gnetum montanum (G.mo)*, *Nicotiana tabacum (N.t.), Oryza sativa (O.s.)*, *Solanum lycopersicum (S.h.)*, *Triticum aestivum (T.a.), Zamia integrifolia (Z.i.)* and *Zea mays (Z.m.)*, was conducted with T-Coffee multiple sequence alignment server and displayed using GeneDoc (http://nrbsc.org/gfx/genedoc), with the conserved residue shading mode.

Figure S11. Phylogenetic analysis of homologous MSP1 proteins in plants.

Homologues sequences to the MSP1 protein were obtained by the Basic Local Alignment Search Tool (BLAST), against the plant genome sequence databases. A phylogeny tree (A) was constructed, using the MAFFT multiple sequence alignment server (Katoh et al., 2017), using the genome sequences of different plant species (bootstrap values for 1,000 bootstrap replicates). These include the *A. thaliana* MSP1 protein (NP_001320003.1, labeled in white), and its putative homologs in different *Brassicaceae*, as well as in *Amygdaloideae*, *Anacardiaceae*, *Betulaceae*, *Citrus*, *Cleomacea*, *Dipterocarpaceae*, *Euphorbiaceae*, *Fabaceae*, *Fagaceae*, *Malvaceae*, *Poaceae*, *Rosoideae*, *Salicaceae*, *Sapindaceae*, *Solanaceae*, *Theaceae* and *Vitaceae*. The graphics at the end of the branches indicate to the specific plant family. (B) Alignment of homologous MSP1 and DEK2 related proteins from *A. thaliana*, *B. rapa*, *B. distachyon*, *H. vulgare*, *J. microsperma*, *N. tabacum*, *O. sativa*, *P. sitchensis*, *P. alba*, *S. lycopersicum*, *T. aestivum* and *Z. mays*, was conducted with T-Coffee multiple sequence alignment server, and displayed using GeneDoc (http://nrbsc.org/gfx/genedoc), with the conserved residue shading mode.

Supplementary Table S1. List of *Arabidopsis PPR-EMB* genes with predicted or established roles in plastid RNA metabolism.

Supplementary Table S2. Lists of oligonucleotides used for the analysis of the splicing profiles of wild-type and mutant plants by RT-qPCR experiments.

Supplementary Table S3. List of splicing factors in *Arabidopsis* and their mtRNA profiles.

Supplementary Table S4. List of antibodies used for the analysis of Col-0 and *msp1* mutants.

Supplementary Table S5. Relative accumulation of mitochondrial proteins in wild-type and *msp1* plants.

Supplementary Table S6. Oligonucleotides used in screening of individual T-DNA insertion lines in *Arabidopsis* and cloning of the *MSP1-GFP* gene-fusion construct.

Supplementary Data S1. mtRNA landscapes of *msp1* mutants.

Total mtRNA extracted from Col-0 and embryo-rescued *msp1-1* plantlets was used to generate Illumina sequencing libraries (BioProjects PRJNA704631 and PRJNA768306). The alignments were visualized using the IGV genome browser (Thorvaldsdottir *et al.*, 2013). Data are shown for the regions corresponding to different organellar transcripts in *Arabidopsis* mitochondria (Best *et al.*, 2020b). Green, blue and red lines point to variation in sequence between the mtRNA (RNA-seq data) and the updated mitogenome sequence of *Arabidopsis* (Sloan *et al.*, 2018).

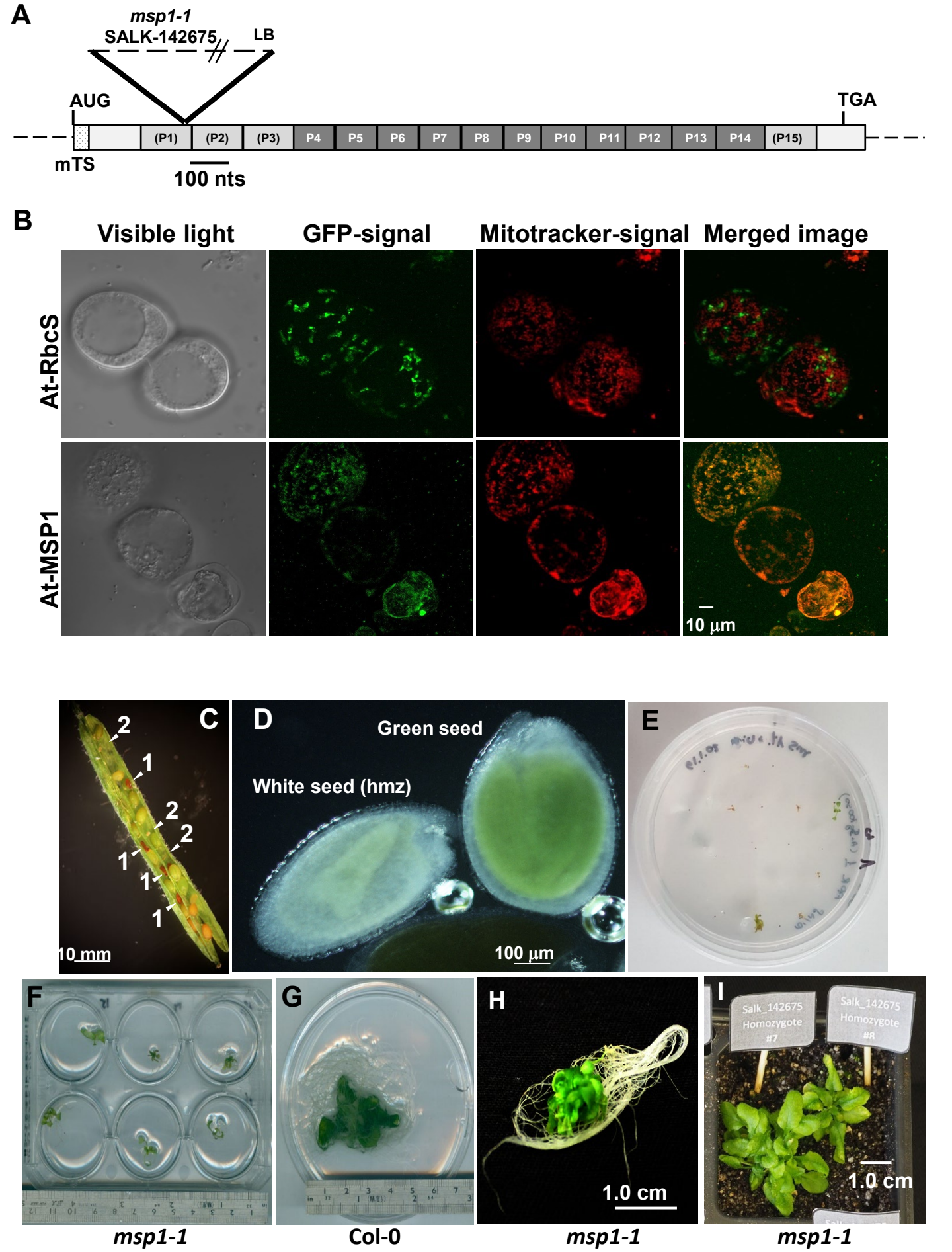
A
msp1-1
SALK-142675
LB
AUG
TGA
(P1)
(P2)
(P3)
P4
P5
P6
P7
P8
P9
P10
P11
P12
P13
P14
(P15)
mTS
100 nts
B
Visible light
GFP-signal
Mitotracker-signal
Merged image
At-RbcS
At-MSP1
10 µm
C
2
1
2
2
1
1
1
10 mm
D
Green seed
White seed (hmz)
100 µm
E
F
G
H
1.0 cm
I
Salk_142675
Homozygote
#7
Salk_142675
Homozygote
#8
1.0 cm
msp1-1
Col-0
msp1-1
msp1-1

Figure 1

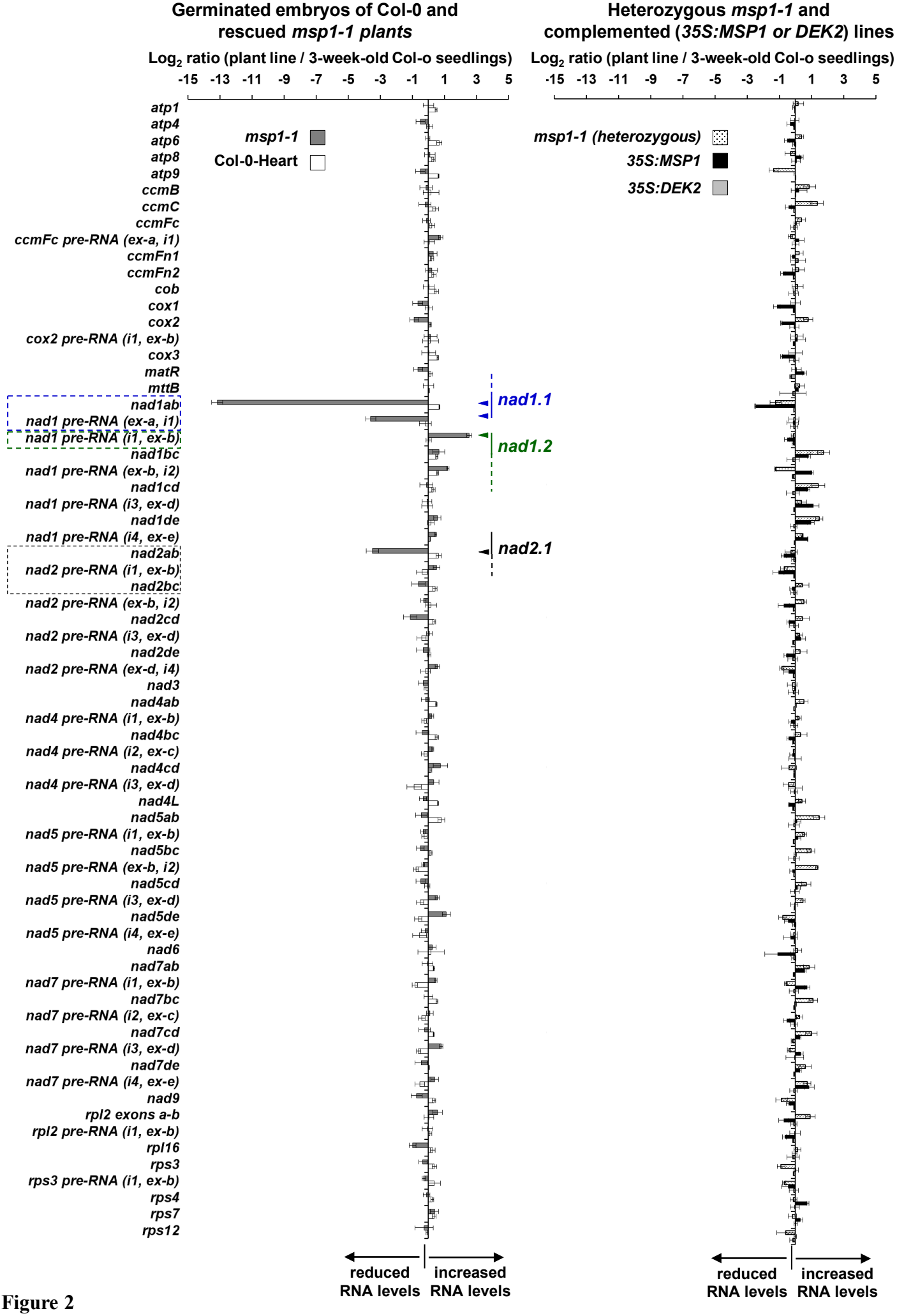
Germinated embryos of Col-0 and rescued msp1-1 plants
Log2 ratio (plant line / 3-week-old Col-o seedlings)
-15 -13 -11 -9 -7 -5 -3 -1 1 3 5
msp1-1
Col-0-Heart
nad1.1
nad1.2
nad2.1
atp1
atp4
atp6
atp8
atp9
ccmB
ccmC
ccmFc
ccmFc pre-RNA (ex-a, i1)
ccmFn1
ccmFn2
cob
cox1
cox2
cox2 pre-RNA (i1, ex-b)
cox3
matR
mttB
nad1ab
nad1 pre-RNA (ex-a, i1)
nad1 pre-RNA (i1, ex-b)
nad1bc
nad1 pre-RNA (ex-b, i2)
nad1cd
nad1 pre-RNA (i3, ex-d)
nad1de
nad1 pre-RNA (i4, ex-e)
nad2ab
nad2 pre-RNA (i1, ex-b)
nad2bc
nad2 pre-RNA (ex-b, i2)
nad2cd
nad2 pre-RNA (i3, ex-d)
nad2de
nad2 pre-RNA (ex-d, i4)
nad3
nad4ab
nad4 pre-RNA (i1, ex-b)
nad4bc
nad4 pre-RNA (i2, ex-c)
nad4cd
nad4 pre-RNA (i3, ex-d)
nad4L
nad5ab
nad5 pre-RNA (i1, ex-b)
nad5bc
nad5 pre-RNA (ex-b, i2)
nad5cd
nad5 pre-RNA (i3, ex-d)
nad5de
nad5 pre-RNA (i4, ex-e)
nad6
nad7ab
nad7 pre-RNA (i1, ex-b)
nad7bc
nad7 pre-RNA (i2, ex-c)
nad7cd
nad7 pre-RNA (i3, ex-d)
nad7de
nad7 pre-RNA (i4, ex-e)
nad9
rpl2 exons a-b
rpl2 pre-RNA (i1, ex-b)
rpl16
rps3
rps3 pre-RNA (i1, ex-b)
rps4
rps7
rps12
reduced RNA levels
increased RNA levels
Heterozygous msp1-1 and complemented (35S:MSP1 or DEK2) lines
Log2 ratio (plant line / 3-week-old Col-o seedlings)
-15 -13 -11 -9 -7 -5 -3 -1 1 3 5
msp1-1 (heterozygous)
35S:MSP1
35S:DEK2
reduced RNA levels
increased RNA levels

Figure 2

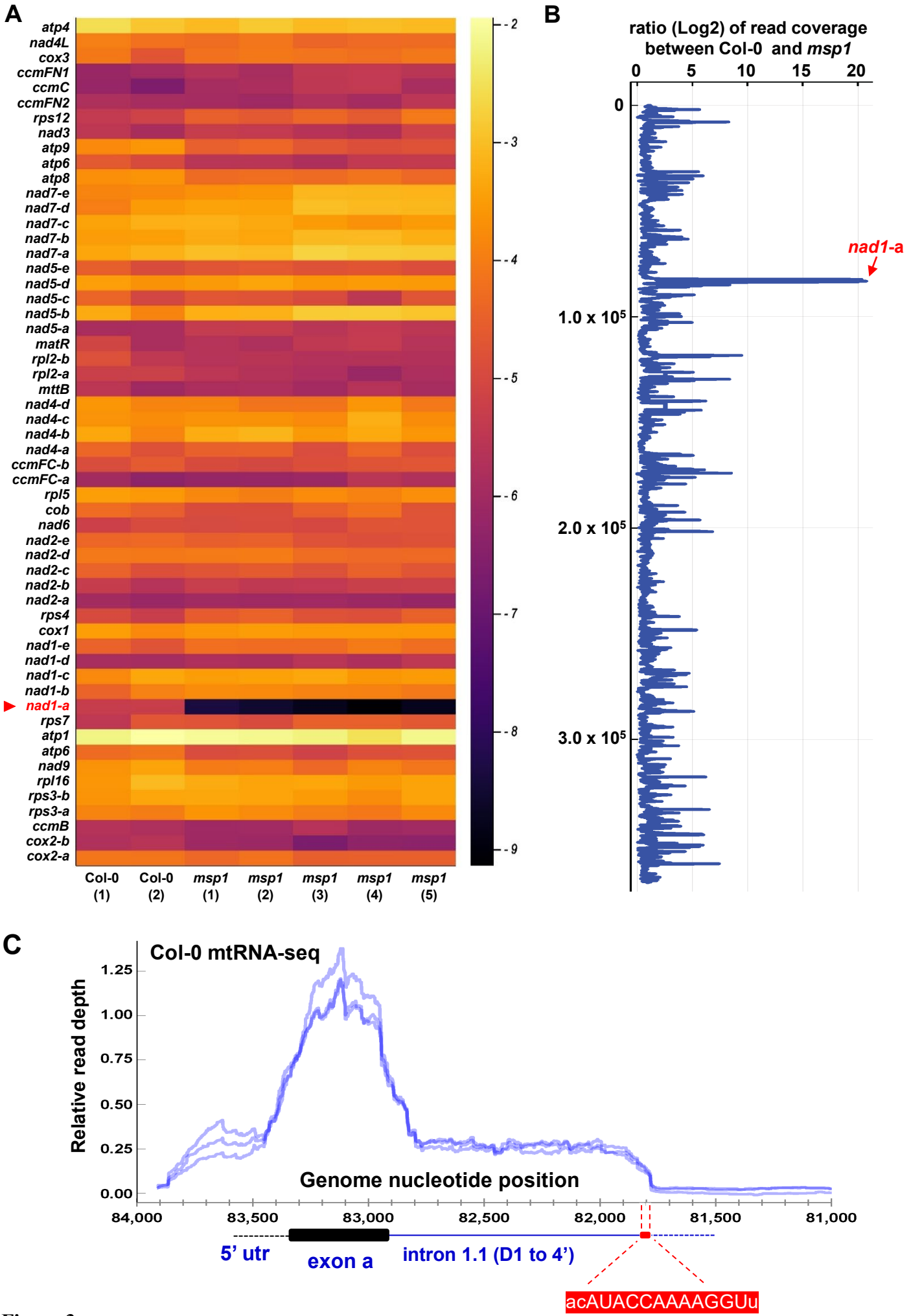
A
atp4
nad4L
cox3
ccmFN1
ccmC
ccmFN2
rps12
nad3
atp9
atp6
atp8
nad7-e
nad7-d
nad7-c
nad7-b
nad7-a
nad5-e
nad5-d
nad5-c
nad5-b
nad5-a
matR
rpl2-b
rpl2-a
mttB
nad4-d
nad4-c
nad4-b
nad4-a
ccmFC-b
ccmFC-a
rpl5
cob
nad6
nad2-e
nad2-d
nad2-c
nad2-b
nad2-a
rps4
cox1
nad1-e
nad1-d
nad1-c
nad1-b
nad1-a
rps7
atp1
atp6
nad9
rpl16
rps3-b
rps3-a
ccmB
cox2-b
cox2-a
Col-0 (1)
Col-0 (2)
msp1 (1)
msp1 (2)
msp1 (3)
msp1 (4)
msp1 (5)
-2
-3
-4
-5
-6
-7
-8
-9
B
ratio (Log2) of read coverage between Col-0 and msp1
0
5
10
15
20
0
1.0 x 10^5
2.0 x 10^5
3.0 x 10^5
nad1-a
C
Col-0 mtRNA-seq
Relative read depth
1.25
1.00
0.75
0.50
0.25
0.00
Genome nucleotide position
84,000
83,500
83,000
82,500
82,000
81,500
81,000
5' utr
exon a
intron 1.1 (D1 to 4')
acAUACCAAAAGGUu

Figure 3

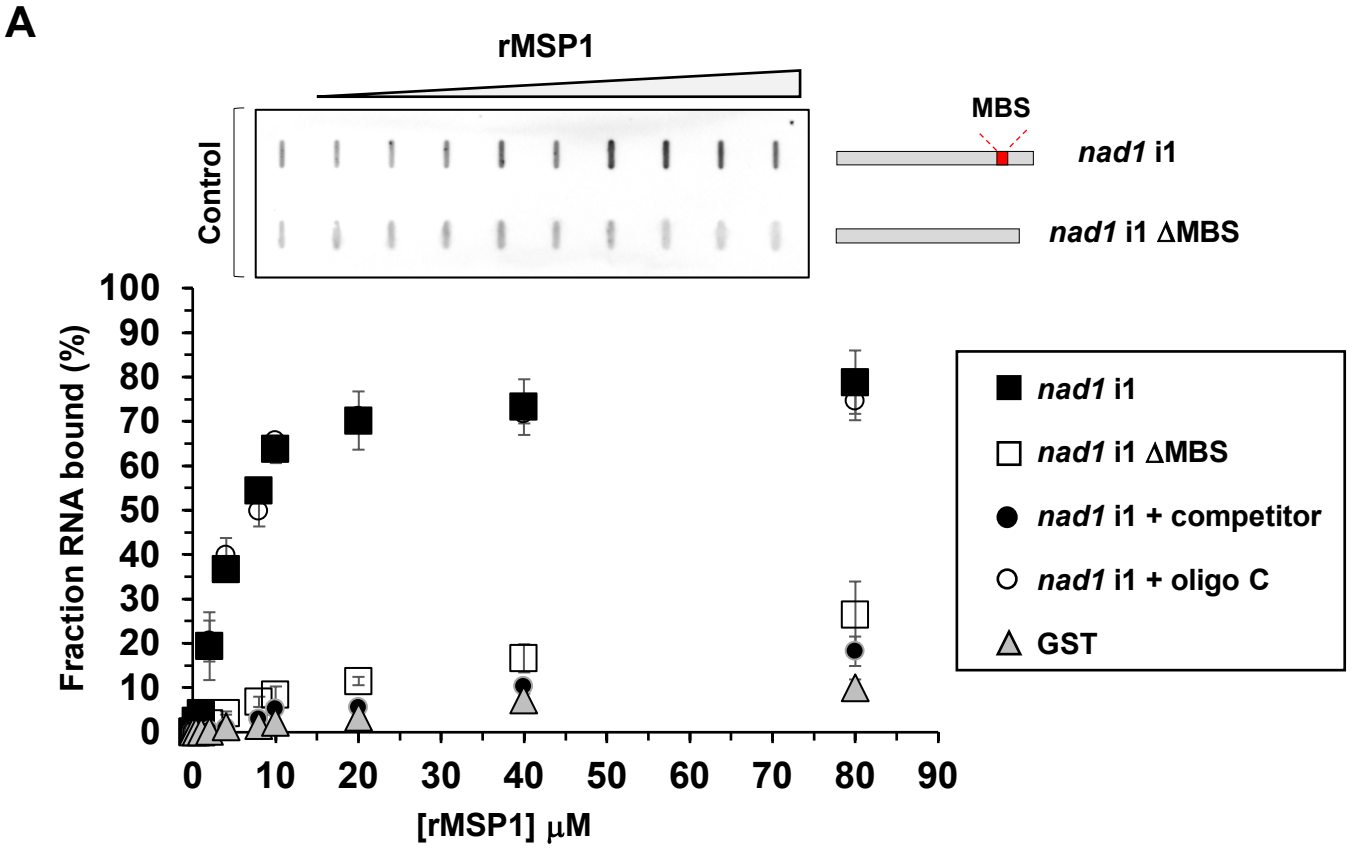
A
rMSP1
Control
MBS
nad1 i1
nad1 i1 ΔMBS
Fraction RNA bound (%)
100
90
80
70
60
50
40
30
20
10
0
0
10
20
30
40
50
60
70
80
90
[rMSP1] μM
nad1 i1
nad1 i1 ΔMBS
nad1 i1 + competitor
nad1 i1 + oligo C
GST

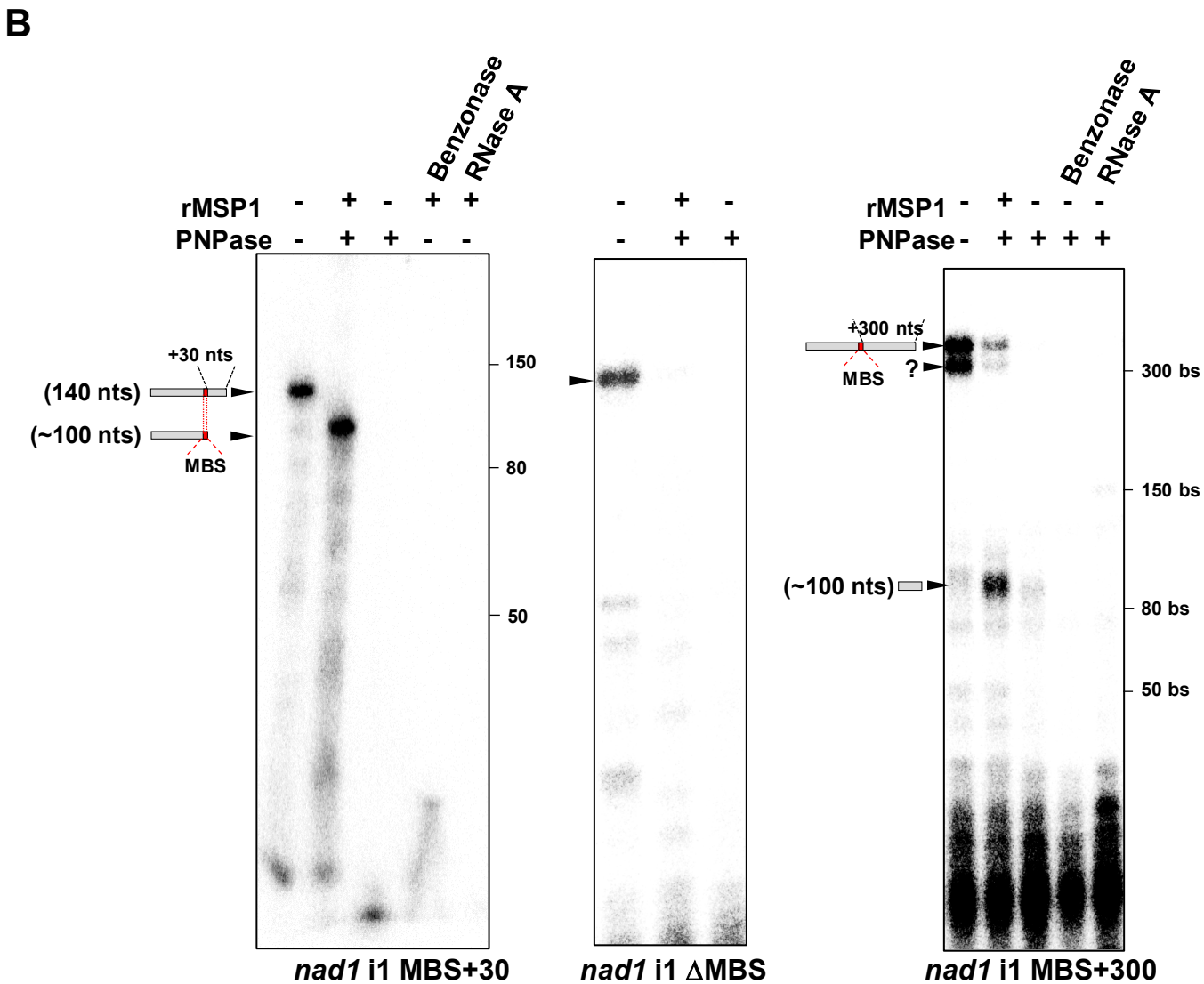
B
Benzonase
RNase A
rMSP1 - + - + +
PNPase - + + - -
+30 nts
(140 nts)
(~100 nts)
MBS
150
80
50
nad1 i1 MBS+30
- + -
- + +
nad1 i1 ΔMBS
Benzonase
RNase A
rMSP1 - + - - -
PNPase - + + + +
+300 nts
MBS
?
(~100 nts)
300 bs
150 bs
80 bs
50 bs
nad1 i1 MBS+300

Figure 4

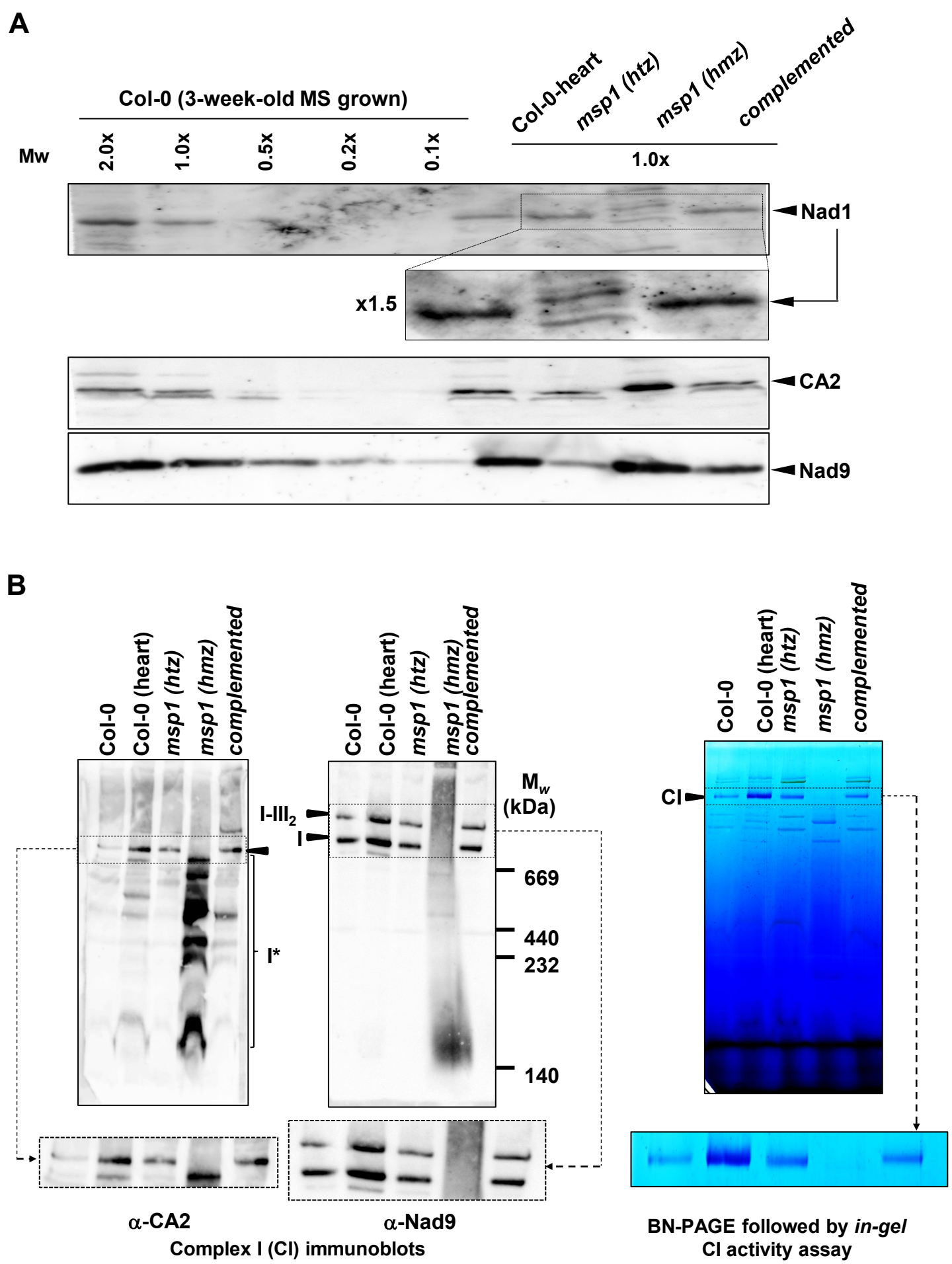
A
Col-0 (3-week-old MS grown)
Mw
2.0x
1.0x
0.5x
0.2x
0.1x
Col-0-heart
msp1 (htz)
msp1 (hmz)
complemented
1.0x
Nad1
x1.5
CA2
Nad9
B
Col-0
Col-0 (heart)
msp1 (htz)
msp1 (hmz)
complemented
I-III2
I
I*
Mw
(kDa)
669
440
232
140
CI
α-CA2
α-Nad9
Complex I (CI) immunoblots
BN-PAGE followed by in-gel
CI activity assay

Figure 5

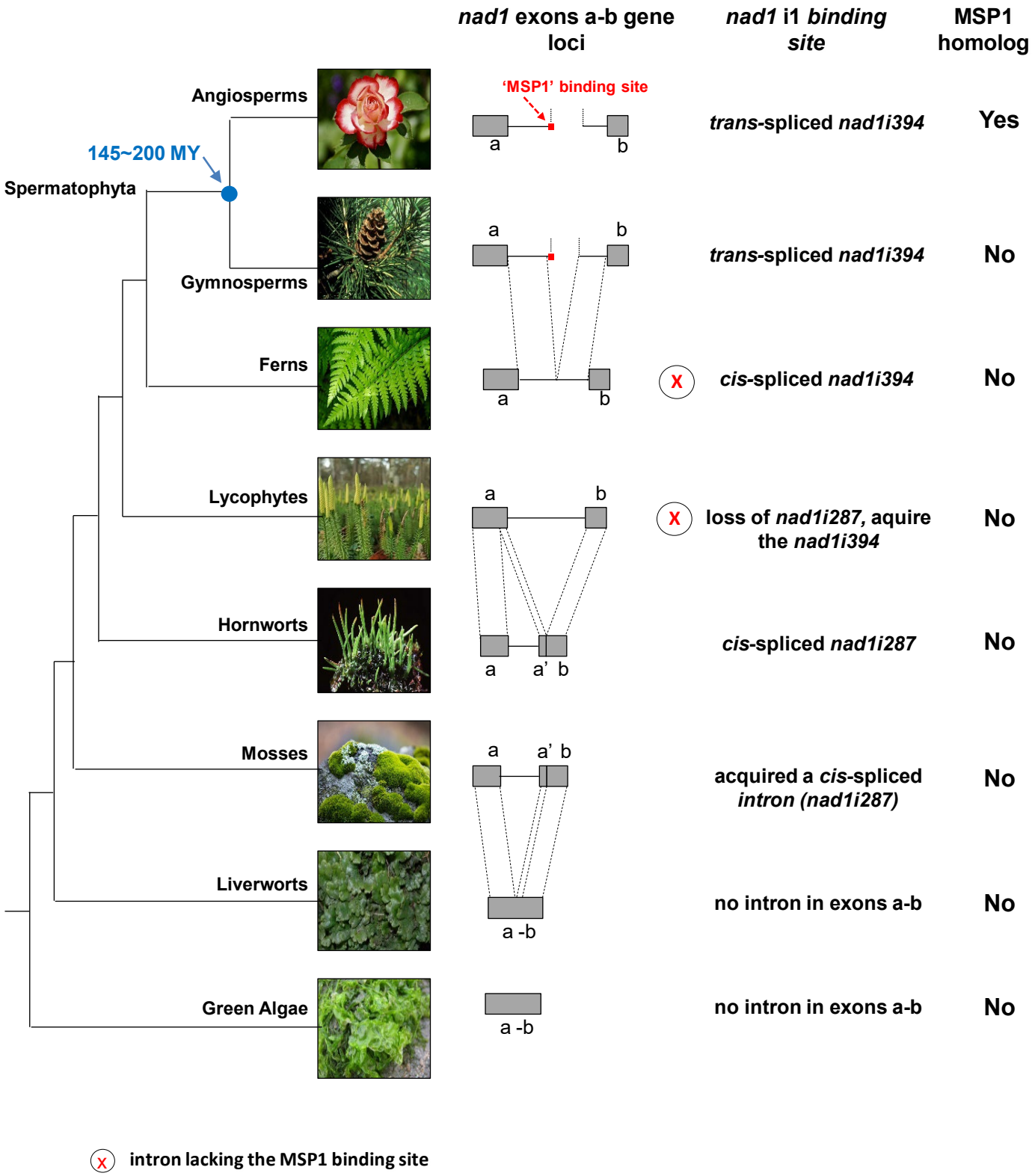
nad1 exons a-b gene loci
nad1 i1 binding site
MSP1 homolog
Angiosperms
145~200 MY
Spermatophyta
Gymnosperms
Ferns
Lycophytes
Hornworts
Mosses
Liverworts
Green Algae
'MSP1' binding site
a
b
trans-spliced nad1i394
Yes
trans-spliced nad1i394
No
cis-spliced nad1i394
No
loss of nad1i287, aquire the nad1i394
No
a'
cis-spliced nad1i287
No
acquired a cis-spliced intron (nad1i287)
No
a -b
no intron in exons a-b
No
no intron in exons a-b
No
X
intron lacking the MSP1 binding site

Figure 6